



Investigation of activation cross-sections of deuteron induced reactions on ruthenium up to 50 MeV



F. Tárkányi ^a, F. Ditrói ^{a,*}, S. Takács ^a, A. Hermanne ^b, A.V. Ignatyuk ^c, I. Spahn ^d, S. Spellerberg ^d

^a Institute for Nuclear Research (ATOMKI), Debrecen, Hungary

^b Cyclotron Laboratory, Vrije Universiteit Brussel (VUB), Brussels, Belgium

^c Institute of Physics and Power Engineering (IPPE), Obninsk, Russia

^d Forschungszentrum Jülich, Institute of Neuroscience and Medicine, Nuclear Chemistry (INM-5), Jülich, Germany

ARTICLE INFO

Keywords:

Deuteron irradiation
Ruthenium target
Rh, Ru and Tc radioisotopes
Cross section
Yield
Medical isotopes

ABSTRACT

The activation cross sections of deuteron induced reactions on natural ruthenium have been measured up to 50 MeV for production of radioisotopes of rhodium (^{105}Rh , ^{102m}Rh , ^{102g}Rh , ^{101m}Rh , ^{101g}Rh , ^{100g}Rh , ^{99m}Rh , ^{99g}Rh), ruthenium (^{105}Ru , ^{103}Ru (cum), ^{102}Ru (cum), ^{97}Ru (cum), ^{95}Ru (cum)) and of technetium (^{99m}Tc , ^{96g}Tc (m+), ^{95m}Tc (cum), ^{95g}Tc (cum), ^{94g}Tc , ^{93g}Tc (m+)). The results are compared with the predictions of the most common theoretical nuclear reaction model codes (ALICE-D, EMPIRE-D and TALYS (TENDL)). From the measured cross section physical yields have been calculated for all measured radioisotopes. The medically important radioisotopes are discussed from the point of view of production routes by charged particle methods and other alternatives.

1. Introduction

We are performing a systematic investigation on activation cross sections of deuteron induced nuclear reactions in all elements. The investigation up till now covered around 1200 excitation functions for reactions on 61 elements (natural targets or enriched stable isotopes). The investigation is connected to projects in a wide range of subjects as activation analyses, medical isotope production, radiation safety of accelerator elements, nuclear reaction theory, etc. In the present work we investigated the activation cross sections of deuteron induced reactions on ruthenium up to 50 MeV incident energy. In literature only one experimental study by Mito et al., (1969) (Mito et al., 1969) was found, presenting the cross sections up to 14 MeV for (d,p) reactions on individual stable ^{96}Ru , ^{102}Ru and ^{104}Ru isotopes, although natural ruthenium targets were used, and an unpublished PhD work (Sitarz et al., 2019) providing data for some radioisotopes below 20 MeV. The fission products ^{103}Ru (39.35 d) and especially ^{106}Ru (368 d) are considered troublesome in the PUREX reprocessing process of spent nuclear fuel, but also have, together with some light ion induced reactions (direct or decay) products applications in nuclear medicine (^{106}Ru brachytherapy, ^{105}Rh therapeutic, $^{103}\text{Ru}/^{103m}\text{Rh}$ Auger-electron therapy, ^{101}Rh brachytherapy, ^{97}Ru SPECT, ^{99m}Tc SPECT, ^{94m}Tc PET).

2. Experiment and data evaluation

For measurement of the cross-section data the well-established activation method, using stacked-foil target technique and off-line gamma-ray spectroscopy, was used. The preparation of the thin samples used for the performed cross section measurements was achieved using the sedimentation technique (Rosch et al., 1993). In this process salt of ruthenium, namely RuCl_3 (99.9%, Carl-Roth Karlsruhe) was suspended in wet ethanol and transferred into Teflon sedimentation cells equipped with aluminum foils of 0.05 mm thickness and 13 mm diameter as backing for the sediments. After evaporation of the liquid the dried samples were each covered with aluminum foils of 0.01 mm thickness. The target was covered by a 10 μm Al foil for protection. The thickness of the sediment layer was 5–45 mg/cm^2 RuCl_3 . Reactions on the Al backing and the Al cover served as monitor.

The target stack was irradiated in a Faraday cup-like target holder equipped with a 5 mm collimator. The details of the experimental technique, spectra evaluation and cross section determination are collected in Table 1. The used decay data are collected in Table 2. Effective beam intensities and the energy scale were determined by using the excitation functions of the ^{24}Al (d,x) ^{24}Na reaction, simultaneously re-measured over the whole energy range. For illustration, the excitation functions of this monitor reaction, in comparison with the

* Corresponding author.

E-mail address: ditroi@atomki.hu (F. Ditrói).

Table 1

Main experimental parameters and data evaluation.

Experimental parameters		Data evaluation	
Incident particle	deuteron	Gamma spectra evaluation	Genie 2000 (Canberra, 2000)
Method	Stacked foil	Determination of beam intensity	Forgamma (Székely, 1985)
Target and thickness (μm)	Ruthenium chloride, 99.9% sedimented 5.5–43.7 mg/cm ²	Decay data	Faraday cup (preliminary) Fitted monitor reaction (final) (Tárkányi et al., 1991)
Number of RuCl ₃ target samples	25	Reaction Q-values	NUDAT 2.8 (Laboratory, 2019)
Stack composition and thickness (μm)	Al (10 μm) Rb ₂ SO ₄ (126.5–7.4 μm) Al (50 μm) Al (10 μm) RuCl ₃ (134.8–16.9 μm) Al (50 μm) repeated 19 times + Ti (22 μm) Al (10 mm) Rb ₂ SO ₄ (126.5–7.4 mm) Al (50 mm) Al (10 μm) RuCl ₃ (134.8–16.9 μm) Al (50 μm) repeated 6 times	Determination of beam energy	Andersen (preliminary) (Andersen and Ziegler, 1977) Fitted monitor reaction (final) (Tárkányi et al., 2001)
Accelerator	Cyclone 90 cyclotron of the Université Catholique in Louvain la Neuve (LLN)	Uncertainty of energy	Cumulative effects of possible uncertainties
Primary energy (MeV)	50	Cross sections	Elemental cross section
Energy range (MeV)	48.7–9.7	Uncertainty of cross sections	Sum in quadrature of all individual linear contributions (
Irradiation time (min)	40	Yield	International-Bureau-of-Weights-and-Measures, 1993)
Beam current (nA)	27		Physical yield (Bonardi, 1987 ; Otuka and Takacs, 2015)
Monitor reaction, [recommended values]	²⁷ Al (d,x) ²⁴ Na reaction (Tárkányi et al., 2001)		
Monitor target and thickness (μm)	^{nat} Al (50 + 10)		
detector	HPGe		
γ-spectra measurements	5 series, decreasing distance		
Cooling times (h)	5.5–9.1		
After EOB	21.7–29.0 71.6–146.5 409.2–817.9 3989.9–4490.6		

IAEA recommended data ([Tárkányi et al., 2001](#)) are shown in Fig. 1. The final energy scale was adjusted to the fitted monitor reaction.

For estimation of the uncertainty of the effective beam energy in the target foils, cumulative effects of possible uncertainties in primary energy and target thickness were taken into account together with the effect of the energy straggling and of the correction for the monitor reaction. The uncertainties of cross sections were obtained from the sum in quadrature of all individual contributions (beam current (7%), beam-loss corrections (maximum 1.5%), target thickness (3%), detector efficiency (5%), photo peak area determination and counting statistics 1–20%) ([International-Bureau-of-Weights-and-Measures, 1993](#)). The uncertainty of the non-linear contributing processes like irradiation, cooling and measuring time, and half-life was not considered.

When complex particles are emitted instead of individual protons and neutrons the Q-values have to be decreased by the respective binding energies of the compound particles: np-d, +2.2 MeV; 2np-t, +8.48 MeV; n2p-3 He, +7.72 MeV; 2n2p-a, +28.30 MeV. Isotopic abundances: ⁹⁶Ru (5.54%), ⁹⁸Ru (1.87%), ⁹⁹Ru (12.76%), ¹⁰⁰Ru (12.60%), ¹⁰¹Ru (17.06%), ¹⁰²Ru (31.55%), ¹⁰⁴Ru (18.62%).

3. Nuclear model calculation

The cross sections of the investigated reactions were calculated using the modified pre-compound model codes (versions D) ALICE-IPPE ([Dityuk et al., 1998](#)) and EMPIRE-II ([Herman et al., 2007](#)). The experimental data are also compared with the cross section data in the TENDL-2019 ([Koning et al., 2019](#)) nuclear reaction data library. The TENDL-2019 is based on both default and adjusted TALYS ([Koning and Rochman, 2012](#)) calculations. Also the TENDL-2017 ([Koning et al., 2017](#)) results are shown that are only marginally different.

During the recent analyses of the (d,p) reactions on many elements we were confronted with a large underestimation of the measured cross

sections. We come to the conclusion that the experimentally observed cross sections of the (d,p) reaction cannot be reproduced below 20–30 MeV with the available statistical model codes. It is well known that for the (d,p) reactions at low energies the direct stripping process plays a very important role.

To achieve now a better description of available data, the versions ALIC-IPPE-D and EMPIRE-II-D are used where a phenomenological enhancement factor K in these relations was taken as energy dependent and was estimated to describe the whole set of the observed (d,p) cross sections for medium and heavy nuclei. The direct (d,p) channel is strongly increased through this adaptation and this is reflected in changes for all other reaction channels in both codes.

As ALICE-IPPE calculates only the total cross section, for estimation of isomeric states from the ALICE code the isomeric ratios calculated by EMPIRE-D were applied.

4. Results

The measured experimental cross-section data are shown in Figs. 2–19 together with the predictions of the theoretical models and the results of the earlier measurement found in [Mito et al. \(1969\)](#). The calculated data are presented up to 70 MeV to illustrate the tendencies and the predictivity of the model calculations. The numerical values of the new experimental results are presented in Tables 3 and 4.

4.1. Cross sections of residual radionuclides of rhodium

The radioisotopes of rhodium are produced only by direct (d,xn) reactions. The contributing reactions and the reaction Q-values are presented in Table 2.

Table 2Decay characteristics of the investigated reaction products. (main γ -lines used for evaluation are in bold).

Nuclide Spin Isomeric level	Half-life	Decay path? (%)	E_γ (keV)	I_γ (%)	Contributing process	Q-value (keV)
^{105}Rh $7/2+$	35.36 h	β^- : 100	306.1 318.9	5.1 19.1	^{104}Ru (d,n)	4820.0
$^{102\text{m}}\text{Rh}$ $6+$ 140.7 keV	3.742 y	IT: 0.233 ϵ : 99.767	418.52 475.06 631.29 697.49 766.84 1046.59 1112.8	9.4 95. 56. 44.0 34.0 34.0 19.0	^{101}Ru (d,n) ^{102}Ru (d,2n) ^{104}Ru (d,4n)	3890.0 -5330.0 -20462.0
$^{102\text{g}}\text{Rh}$ $1-,2-$	207.3 d	β^- : 22 ϵ : 78	468.58 556.60 475.06	2.9 2.0 46	^{101}Ru (d,n) ^{102}Ru (d,2n) ^{104}Ru (d,4n)	3890.0 -5330.0 -20462.0
$^{101\text{m}}\text{Rh}$ $9/2+$ 157.32	4.34 d	IT: 7.20 ϵ : 92.8	306.857 545.117	81 4.3	^{100}Ru (d,n) ^{101}Ru (d,2n) ^{102}Ru (d,3n) ^{104}Ru (d,5n)	3249.0 -3553.0 -12772.0 -27904.0
$^{101\text{s}}\text{Rh}$ $1/2-$	3.3 y	ϵ : 100	127.226 198.01 325.23	68 73 11.8	^{100}Ru (d,n) ^{101}Ru (d,2n) ^{102}Ru (d,3n) ^{104}Ru (d,5n)	3249.0 -3553.0 -12772.0 -27904.0
$^{100\text{g}}\text{Rh}$ $1-$	20.8 h	ϵ : 96.1 β^+ : 3.9	446.153 539.512 822.654 1107.223	11.98 80.6 21.09 13.57	^{99}Ru (d,n) ^{100}Ru (d,2n) ^{101}Ru (d,3n) ^{102}Ru (d,4n) ^{104}Ru (d,6n)	3030.0 -6643.0 -13445.0 -22665.0 -37797.0
$^{99\text{m}}\text{Rh}$ $9/2+$ 64.34 keV	4.7 h	ϵ : 94.4 β^+ : 5.6	340.8 617.8 1261.2	72.0 12.3 11.4	^{98}Ru (d,n) ^{99}Ru (d,2n) ^{100}Ru (d,3n) ^{101}Ru (d,4n) ^{102}Ru (d,5n) ^{104}Ru (d,7n)	2421.0 -5051.0 -14724.0 -21526.0 -30746.0 -45878.0
$^{99\text{g}}\text{Rh}$ $1/2-$	16.1 d	β^+ : 100	89.76 353.05 528.24	33.4 34.5 37.9	^{98}Ru (d,n) ^{99}Ru (d,2n) ^{100}Ru (d,3n) ^{101}Ru (d,4n) ^{102}Ru (d,5n) ^{104}Ru (d,7n)	2421.0 -5051.0 -14724.0 -21526.0 -30746.0 -45878.0
^{105}Ru $3/2+$	4.44 h	β^- : 100	129.782 316.44 469.37 676.36 724.30	5.68 11.1 17.5 15.7 47.3	^{102}Ru (d,p) ^{104}Ru (d,p2n)	3685.53
^{103}Ru $3/2+$	39.247 d	β^- : 100	497.085	91.0	^{96}Ru (d,p) ^{98}Ru (d,p2n)	4007.48 -11124.0
^{97}Ru $5/2+$	2.83 d	ϵ : 100	215.70 324.49	85.62 10.79	^{98}Ru (d,p2n) ^{99}Ru (d,p3n) ^{100}Ru (d,p4n) ^{101}Ru (d,p5n) ^{102}Ru (d,p6n) ^{104}Ru (d,p8n)	5887.0 -12400.0 -19872.0 -29545.0 -36347.0 -45567.0 -60699.0
^{95}Ru $5/2+$	1.643 h	ϵ : 100	336.40 626.83 1096.80	69.9 17.8 20.9	^{97}Rh decay ^{98}Ru (d,p2n) ^{98}Ru (d,p4n) ^{99}Ru (d,p5n) ^{100}Ru (d,p6n) ^{101}Ru (d,p7n) ^{102}Ru (d,p8n) ^{104}Ru (d,p10n)	-12919.0 -31206.0 -38677.0 -48351.0 -55153.0 -64372.0 -55200.0
$^{99\text{m}}\text{Tc}$ $1/2-$	6.0072 h	β^- : 0.0037 IT: 99.9963	140.511	89	^{95}Rh decay ^{99}Ru (d,2p) ^{100}Ru (d,2pn) ^{101}Ru (d,2p2n) ^{102}Ru (d,2p3n) ^{104}Ru (d,2p5n)	-1739.7 -11413.1 -18215.1 -27434.7 -42567.0
$^{96\text{g}}\text{Tc}$ $7+$	4.28 d	ϵ : 100	778.22 812.54 849.86 1126.85	99.760 82 98 15.2	^{96}Ru (d,2p) ^{98}Ru (d,2p2n) ^{99}Ru (d,2p3n) ^{100}Ru (d,2p4n) ^{101}Ru (d,2p5n) ^{102}Ru (d,2p6n) ^{104}Ru (d,2p8n)	-1701.0 -19988.0 -27460.0 -37133.0 -43935.0 -53155.0 -68287.0

(continued on next page)

Table 2 (continued)

Nuclide Spin Isomeric level	Half-life	Decay path? (%)	E_{γ} (keV)	I_{γ} (%)	Contributing process	Q-value (keV)
^{95m} Tc 1/2- 38.914 keV	61 d	ε : 96.12 IT: 3.88	204.117 582.082 835.149	63.2 30.0 26.6	⁹⁶ Ru (d,2pn) ⁹⁸ Ru (d,2p3n) ⁹⁹ Ru (d,2p4n) ¹⁰⁰ Ru (d,2p5n) ¹⁰¹ Ru (d,2p6n) ¹⁰² Ru (d,2p7n) ¹⁰⁴ Ru (d,2p9n) ⁹⁶ Ru (d,2pn) ⁹⁸ Ru (d,2p3n) ⁹⁹ Ru (d,2p4n) ¹⁰⁰ Ru (d,2p5n) ¹⁰¹ Ru (d,2p6n) ¹⁰² Ru (d,2p7n) ¹⁰⁴ Ru (d,2p9n) ⁹⁵ Ru decay	-9573.0 -27860.0 -35332.0 -45005.0 -51807.0 -61027.0 -76158.0 -9573.0 -27860.0 -35332.0 -45005.0 -51807.0 -61027.0 -76158.0
^{95g} Tc 9/2+	20.0 h	ε : 100	765.789 1073.71	93.8 3.74	⁹⁶ Ru (d,2pn) ⁹⁸ Ru (d,2p3n) ⁹⁹ Ru (d,2p4n) ¹⁰⁰ Ru (d,2p5n) ¹⁰¹ Ru (d,2p6n) ¹⁰² Ru (d,2p7n) ¹⁰⁴ Ru (d,2p9n) ⁹⁵ Ru decay	-9573.0 -27860.0 -35332.0 -45005.0 -51807.0 -61027.0 -76158.0
^{94m} Tc (2)+ 763	52.0 min	ε : 100	871.05 993.19 1522.1	94.2 2.21 4.5	⁹⁶ Ru (d,2p2n) ⁹⁸ Ru (d,2p4n) ⁹⁹ Ru (d,2p5n) ¹⁰⁰ Ru (d,2p6n) ¹⁰¹ Ru (d,2p7n) ¹⁰² Ru (d,2p8n) ¹⁰⁴ Ru (d,2p10n) ⁹⁴ Ru decay	-19507.0 -37794.0 -45266.0 -54939.0 -61741.0 -70961.0
^{94g} Tc 7+	293 min	ε : 100	449.2 702.67 849.74 871.05 916.10	3.3 99.6 95.7 99.9 7.6	⁹⁶ Ru (d,2p2n) ⁹⁸ Ru (d,2p4n) ⁹⁹ Ru (d,2p5n) ¹⁰⁰ Ru (d,2p6n) ¹⁰¹ Ru (d,2p7n) ¹⁰² Ru (d,2p8n) ¹⁰⁴ Ru (d,2p10n) ⁹⁴ Ru decay	-19507.0 -37794.0 -45266.0 -54939.0 -61741.0 -70961.0
⁹³ Tc 9/2+	2.75 h	ε : 100	1362.94 1520.28	66.2 24.4	⁹⁶ Ru (d,2p3n) ⁹⁸ Ru (d,2p5n) ⁹⁹ Ru (d,2p6n) ¹⁰⁰ Ru (d,2p7n) ¹⁰¹ Ru (d,2p8n) ¹⁰² Ru (d,2p9n) ¹⁰⁴ Ru (d,2p11n) ⁹³ Ru decay	-28130.4 -46418.0 -53889.4 -63562.7 -70364.8 -79584.4

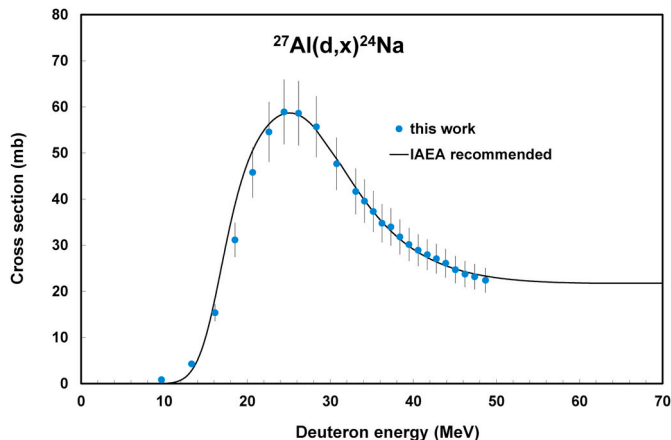


Fig. 1. Excitation function of the simultaneously irradiated $^{27}\text{Al}(\text{d},\text{x})^{24}\text{Na}$ monitor reaction, in comparison with IAEA recommended values (Tárkányi et al., 2001).

4.1.1. The $^{\text{nat}}\text{Ru}(\text{d},\text{xn})^{105}\text{Rh}$ process

The 35.36 h half-life ^{105}Rh decays for 100% with β^- to stable ^{105}Pd . The production cross sections of the ^{105}Rh are cumulative as they are measured after complete decay of ^{105}Ru (4.44 h half-life, β : 100%), and are shown in Fig. 2, together with theoretical estimations. Above 18 MeV the best estimation is given by the EMPIRE-D, but it strongly

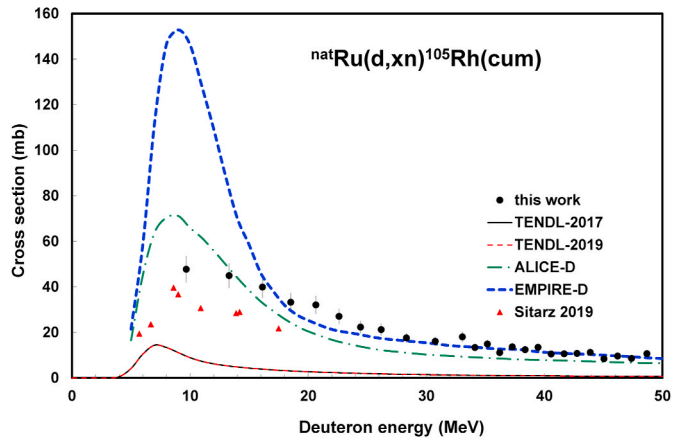


Fig. 2. Experimental excitation functions of the $^{\text{nat}}\text{Ru}(\text{d},\text{xn})^{105}\text{Rh}$ reaction in comparison with theoretical results.

overestimates around the maximum. The cross section peak could not be reconstructed by our measurement but the prediction of ALICE-D is the best around the peak energy. Both TENDL versions strongly underestimate in the whole energy region and they give the same result. The only experimental results at low energies are obviously lower than ours.

4.1.2. The $^{\text{nat}}\text{Ru}(\text{d},\text{xn})^{102m}\text{Rh}$ process

The 3.742 y half-life isomeric state decays for 0.233% by IT to the

Table 3

Cross sections of deuteron induced reactions on ruthenium for production of rhodium radioisotopes.

E MeV	dE	^{105}Rh		$^{102\text{m}}\text{Rh}$		$^{102\text{g}}\text{Rh}$		$^{101\text{m}}\text{Rh}$		$^{101\text{g}}\text{Rh}$		$^{100\text{g}}\text{Rh}$		$^{99\text{m}}\text{Rh}$		$^{99\text{g}}\text{Rh}$	
		σ mb	$d\sigma$	σ	$d\sigma$	σ	$d\sigma$	σ	$d\sigma$								
48.69	0.30	10.66	1.33			43.00	5.14	136.65	16.29	69.44	8.28	141.09	16.82	137.56	16.55	37.15	4.44
47.38	0.37	8.57	1.10	37.52	10.90	43.83	5.24	131.56	15.68	64.14	7.69	147.12	17.55	142.14	17.18	33.61	4.06
46.21	0.39	9.61	1.15	50.07	9.08	47.89	5.76	132.67	15.81	52.83	6.46	154.62	18.44	131.28	15.79	35.03	4.18
45.05	0.42	8.40	1.06	53.24	7.68	44.42	5.35	114.44	13.64	48.74	5.99	143.34	17.10	114.59	13.81	30.49	3.68
43.89	0.45	11.21	1.38			56.19	6.73	132.90	15.84	53.49	6.48	186.34	22.22	130.93	15.78	34.40	4.12
42.77	0.48	10.77	1.35	71.67	9.89	60.28	7.23	128.85	15.36	52.67	6.41	191.41	22.83	122.76	14.82	34.47	4.12
41.67	0.51	10.61	1.32	81.51	10.93	66.18	7.94	121.73	14.51	58.52	7.09	203.68	24.29	122.11	14.78	33.84	4.12
40.57	0.54	10.48	1.32	81.21	12.31			116.98	13.94			207.58	24.76	114.96	13.93	22.06	2.66
39.47	0.56	13.46	1.65	90.01	13.14	70.69	8.44	123.77	14.75	42.57	5.14	232.76	27.76	119.55	14.45	35.47	4.31
38.37	0.59	12.42	1.54					123.37	14.70			234.19	27.93	110.12	13.49	32.72	3.93
37.28	0.62	13.63	1.69	99.47	17.95	83.94	10.02	125.97	15.02	49.37	6.16	238.93	28.50	120.26	14.69	34.06	4.18
36.22	0.64	11.10	1.33	75.56	17.23	63.67	7.62	106.72	12.72	39.09	4.77	190.36	22.72	97.22	11.89	27.34	3.27
35.17	0.67	14.91	1.79	0.00	0.00	83.27	9.96	146.16	17.42	51.33	6.22	244.71	29.20	128.29	15.82	37.79	4.51
34.12	0.70	13.37	1.69	100.71	17.85	80.35	9.68	145.34	17.33	78.25	9.66	218.37	26.06	120.35	14.87	32.92	4.07
33.06	0.72	18.01	2.27	96.59	14.99	78.03	9.34	164.32	19.59	55.50	6.75	213.35	25.45	123.03	15.38	33.49	4.05
30.76	0.78	16.07	1.97	79.55	12.98	76.93	9.21	207.18	24.69	87.12	10.47	192.82	23.01	113.24	14.57	21.81	2.74
28.32	0.84	17.57	2.17	55.73	11.41	62.85	7.59	258.96	30.86	100.90	12.28	178.80	21.34	108.00	13.54	33.37	4.04
26.18	0.90	21.24	2.64	49.12	9.77	54.28	6.55	273.13	32.56	110.22	13.34	181.78	21.72	98.92	12.48	33.08	4.13
24.43	0.94	22.31	2.77			56.04	6.78	249.57	29.75	101.34	12.37	166.11	19.85	85.81	11.70	33.10	4.01
22.61	0.98	27.04	3.41	58.38	17.32	70.77	8.51	240.67	28.70	107.84	13.07	167.57	20.04	87.57	11.46	35.60	4.46
20.65	1.03	32.09	3.95	50.45	22.35	93.94	11.26	219.32	26.15	96.57	11.70	159.12	19.04	98.26	12.86	30.28	3.89
18.52	1.09	33.25	4.06			132.94	15.91	190.46	22.71	84.67	10.36	141.40	16.92	75.90	10.14	28.61	3.52
16.13	1.15	39.88	4.77	133.68	22.44	175.57	21.00	147.40	17.57	69.94	8.73	114.15	13.68	69.39	9.18	29.81	3.59
13.30	1.22	44.92	5.37	85.90	15.24	152.48	18.28	105.71	12.60	56.07	7.19	84.32	10.12	56.13	7.44	27.33	3.27
9.67	1.31	47.73	5.78			109.60	15.36	65.48	7.80			49.70	6.03	33.33	4.75	17.35	2.10

207.3 d half-life ground state and for the rest by EC to stable ^{102}Ru . The production cross sections of the $^{102\text{m}}\text{Rh}$ are shown in Fig. 3 together with theoretical estimations. Now the best estimation is given by the ALICE-D in the whole energy region. Both TENDL versions give identical results, mostly overestimate the experimental data and fail in giving the peak positions. The EMPIRE-D overestimates the experimental data.

4.1.3. The ${}^{\text{n}at}\text{Ru}(d,xn)^{102\text{g}}\text{Rh}$ process

The $^{102\text{g}}\text{Rh}$ ($T_{1/2} = 207.3$ d) decays with $\epsilon: 78\%$ and $\beta^-: 22\%$ to stable ^{102}Ru . The experimental data were obtained by subtracting the small contribution of the isomeric state, i.e. direct production cross sections are presented (Fig. 4). Now the best results are given by EMPIRE-D, both ALICE-D and the TENDL underestimate the experimental results.

4.1.4. The ${}^{\text{n}at}\text{Ru}(d,xn)^{101\text{m}}\text{Rh}$ process

The radionuclide ^{101}Rh has two states: a high spin isomer (${}^{101\text{m}}\text{Rh}$, $T_{1/2} = 4.34$ d, IT: 7.20% $\epsilon: 92.8\%$) and the longer-lived ground state (${}^{101\text{g}}\text{Rh}$, $T_{1/2} = 3.3$ y, $\epsilon: 100\%$). We obtained the production cross section of the isomeric state as can be seen in Fig. 5. None of the theoretical model codes give an acceptable estimation now, except the EMPIRE-D predictions between 40 and 50 MeV. The single dataset at low energies (Sitarz, 2019) is slightly lower than our new data.

4.1.5. The ${}^{\text{n}at}\text{Ru}(d,xn)^{101\text{g}}\text{Rh}$ ($m+$) process

The cross section for the ground state formation of $^{101\text{g}}\text{Rh}$ ($T_{1/2} = 3.3$ y), after the complete decay of the isomeric state, is shown in Fig. 6. The experimental data are a bit more scattered here, but one can state that the EMPIRE-D gives the best approximation above 25 MeV while ALICE-D below, which runs almost together with the both TENDL versions under 20 MeV.

4.1.6. The ${}^{\text{n}at}\text{Ru}(d,xn)^{100\text{g}}\text{Rh}$ ($m+$) process

The experimental and theoretical results for production of ground state of ^{100}Rh ($T_{1/2} = 20.8$ h, $\epsilon: 100\%$), obtained after complete decay of short-lived isomeric state ($T_{1/2} = 4.6$ min, IT: 98.3%, $\epsilon: 1.7\%$) are shown in Fig. 7. All theoretical model codes overestimate the experimental results, only the approximation of ALICE-D is acceptable between 43 and

50 MeV. The only literature data (Sitarz, 2019) is slightly lower than ours.

4.1.7. The ${}^{\text{n}at}\text{Ru}(d,xn)^{99\text{m}}\text{Rh}$ process

The radionuclide ^{99}Rh has two long-lived states decaying independently: a shorter-lived, high spin isomer ($T_{1/2} = 4.7$ h, $\epsilon: 100\%$) and the longer-lived ground state ($T_{1/2} = 16.1$ d, $\epsilon > 99.84\%$ IT $< 0.16\%$). We could measure the cross section data for both states separately. The experimental and theoretical results for direct production of the isomeric state are shown in Fig. 8. The theoretical model codes overestimate our experimental data and some of them produce even local maxima, which could not be confirmed by the experiment. A single literature dataset at low energies (Sitarz, 2019) is proved to be lower than ours.

4.1.8. The ${}^{\text{n}at}\text{Ru}(d,xn)^{99\text{g}}\text{Rh}$ process

The experimental and theoretical results for direct production of the ground state ($T_{1/2} = 16.1$ d) are shown in Fig. 9. The theoretical model codes again overestimate the experiment and produce strange local maxima and minima. The available experimental literature data (Sitarz, 2019) is lower than ours.

4.2. Cross sections of residual radionuclides of ruthenium

The radioisotopes of ruthenium are produced by direct (d,pxn) reactions and through the decay of parent radioisotopes. The contributing reactions and the reaction Q-values are presented in Table 2.

4.2.1. The ${}^{\text{n}at}\text{Ru}(d,x)^{105}\text{Ru}$ process

The ^{105}Ru ($T_{1/2} = 4.44$ h, $\beta^-: 100\%$) is produced via the ^{104}Ru (d,p) reaction. The new data are shown in Fig. 10, together with the earlier experimental data (Mito et al., 1969). These literature data, expressed in the original publication as reaction cross sections on single target isotopes, are normalized to natural isotopic contribution. The agreement with the present experiment is satisfactory. Good approximation is given above 20 MeV by ALICE-D, EMPIRE-D and systematics. All theoretical model codes fail in estimation of the peak cross section peak value, while

Table 4

Cross sections of deuteron induced reactions on ruthenium for production of ruthenium and technetium radioisotopes.

E MeV	¹⁰⁵ Ru		¹⁰³ Ru		⁹⁷ Ru		⁹⁵ Ru		^{99m} Tc		^{96g} Tc		^{95m} Tc		^{95g} Tc		^{94g} Tc		⁹³ Tc		
	E	dE	σ	$d\sigma$	σ	$d\sigma$	σ	$d\sigma$	σ	$d\sigma$	σ	$d\sigma$	σ	$d\sigma$	σ	$d\sigma$	σ	$d\sigma$	σ	$d\sigma$	
			mb																		
48.69	0.30	3.80	0.55	65.87	7.85	122.40	14.60	25.28	3.13	4.16	0.51	30.98	3.70	5.64	0.67	50.61	6.04	24.43	2.93	43.73	5.29
47.38	0.37	3.87	0.60	64.07	7.64	116.90	13.94	26.41	3.33	3.94	0.49	27.03	3.24	5.29	0.63	47.83	5.72	24.06	2.89	43.50	5.31
46.21	0.39	4.69	0.63	65.50	7.81	112.90	13.47	23.68	2.85	3.93	0.48	25.45	3.03	5.00	0.61	47.62	5.69	22.61	2.71	24.30	2.95
45.05	0.42	4.61	0.62	58.24	6.95	95.06	11.34	21.03	2.53	3.27	0.40	20.13	2.41	4.56	0.56	39.29	4.70	18.96	2.28	21.58	2.63
43.89	0.45	5.28	0.72	69.45	8.28	110.94	13.24	26.40	3.19	3.77	0.46	23.16	2.77	5.22	0.63	47.16	5.64	21.88	2.63	25.51	3.11
42.77	0.48	6.07	0.81	67.62	8.06	102.36	12.22	25.39	3.08	3.33	0.41	21.56	2.57	4.97	0.60	46.43	5.56	19.98	2.41	27.01	3.30
41.67	0.51	5.81	0.80	71.53	8.53	100.83	12.03	25.70	3.13	3.12	0.39	20.01	2.40	4.87	0.59	45.76	5.48	17.06	2.06	30.95	3.79
40.57	0.54	5.98	0.82			93.36	11.14	27.04	3.28	3.04	0.38	19.14	2.29	0.00	0.00	47.02	5.63	15.81	1.91	28.17	3.45
39.47	0.56	5.38	0.75	67.03	7.99	95.63	11.41	30.89	3.72	3.01	0.38	19.09	2.29	4.50	0.54	51.53	6.17	14.77	1.79	24.98	3.06
38.37	0.59	6.19	0.92			89.10	10.64	32.06	3.99	2.83	0.37	18.69	2.24	0.00	0.00	53.12	6.36	12.89	1.58	50.35	6.17
37.28	0.62	5.65	0.87	0.00	0.00	81.79	9.77	32.25	3.98	2.12	0.29	18.23	2.19	4.88	0.59	53.57	6.42	9.32	1.17	43.66	5.36
36.22	0.64	8.51	1.18	53.50	6.38	63.71	7.62	29.37	3.55	2.35	0.31	14.10	1.68	3.67	0.45	46.79	5.62	7.27	0.91	22.88	2.84
35.17	0.67	9.57	1.37	68.62	8.18	71.67	8.57	39.95	5.02	2.04	0.30	17.27	2.06	4.87	0.59	60.70	7.28	7.45	0.99	57.93	7.15
34.12	0.70	8.04	1.20	67.84	8.10	56.77	6.80	35.01	4.40	2.48	0.35	14.16	1.72	4.82	0.60	54.83	6.59	5.02	0.70	42.55	5.32
33.06	0.72	7.21	1.22	62.17	7.41	50.71	6.08	33.57	4.58	1.36	0.25	13.46	1.63	4.17	0.51	56.33	6.75	2.36	0.48	57.64	7.26
30.76	0.78	12.63	1.81	66.02	7.87	33.48	4.02	35.27	4.43	1.55	0.23	11.43	1.42	4.45	0.55	51.92	6.22	1.53	0.30	44.91	5.55
28.32	0.84	10.87	1.60	64.84	7.74	25.93	3.14	30.41	3.84	1.66	0.29	10.39	1.26	3.79	0.51	45.07	5.42			33.70	4.28
26.18	0.90	13.96	1.94	53.47	6.38	21.36	2.62	23.60	3.02	2.05	0.32	9.81	1.22	2.62	0.35	31.86	3.89	0.83	0.27	27.63	3.61
24.43	0.94	11.65	2.09	46.18	5.51	17.34	2.16	14.57	2.91	1.66	0.33	0.00	0.00	1.80	0.27	21.62	2.68			46.32	6.16
22.61	0.98	16.27	2.30	43.39	5.18	13.90	1.78	9.88	1.83	1.88	0.33	8.17	1.05	1.58	0.25	13.37	1.76			41.72	5.35
20.65	1.03	19.32	2.74	42.42	5.06	12.50	1.63			1.70	0.32	7.31	0.95	0.43	0.14	6.11	0.96			37.29	5.04
18.52	1.09	16.97	2.40	44.71	5.34	11.71	1.52			1.63	0.32	0.00	0.00			1.14	0.36			30.91	4.17
16.13	1.15	23.69	3.09	51.84	6.19	15.25	1.91					3.50	0.43							19.95	2.81
13.30	1.22	28.91	3.66	54.83	6.55	19.12	2.35					1.45	0.18			0.53	0.16			12.59	1.91
9.67	1.31	32.80	4.12	72.49	8.77	21.06	2.59					0.42	0.06							4.61	0.92

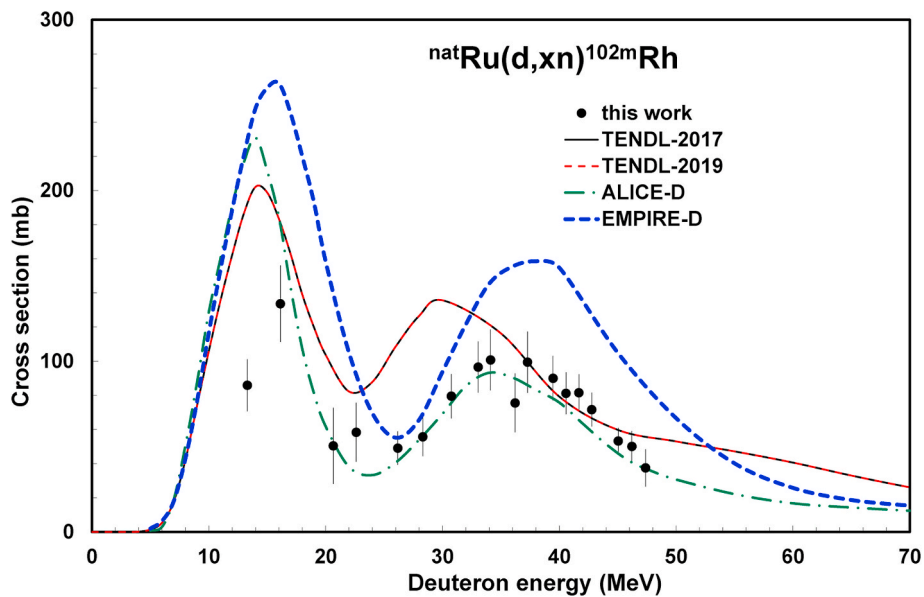


Fig. 3. Experimental excitation functions of the $^{nat}\text{Ru}(d, xn)^{102m}\text{Rh}$ reaction in comparison with theoretical results.

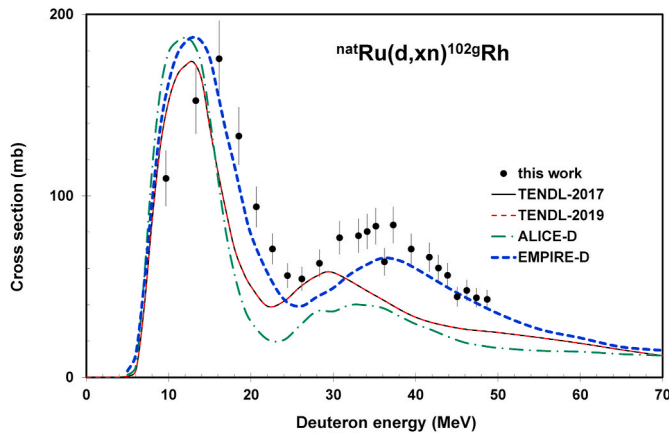


Fig. 4. Experimental excitation function of the $^{nat}\text{Ru}(d, xn)^{102g}\text{Rh}$ reaction in comparison with theoretical results.

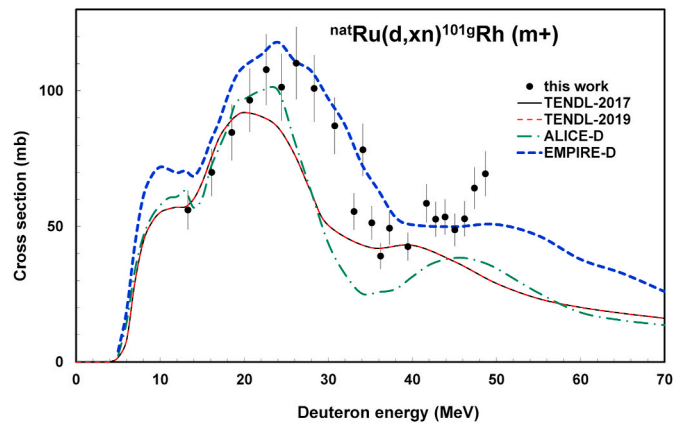


Fig. 6. Experimental excitation function of the $^{nat}\text{Ru}(d, xn)^{101g}\text{Rh}$ reaction in comparison with theoretical results.

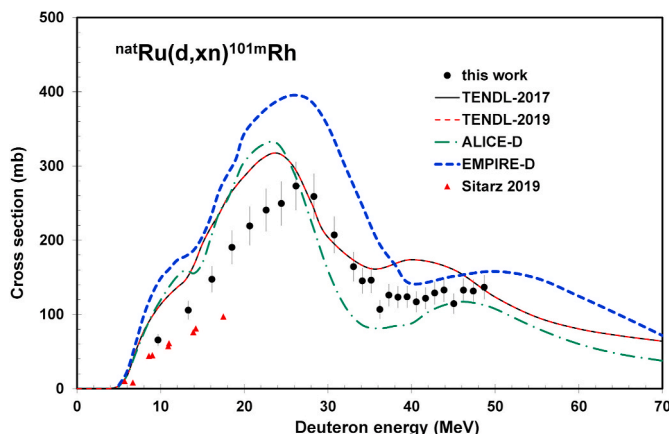


Fig. 5. Experimental excitation function of the $^{nat}\text{Ru}(d, xn)^{101m}\text{Rh}$ reaction in comparison with theoretical results.

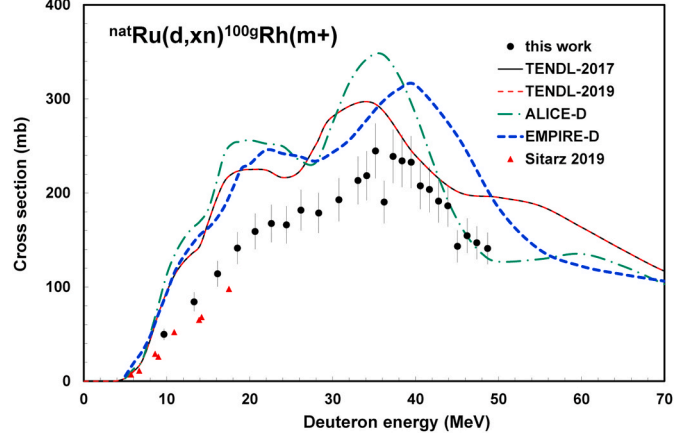


Fig. 7. Experimental excitation function of the $^{nat}\text{Ru}(d, xn)^{100g}\text{Rh}$ reaction in comparison with theoretical results.

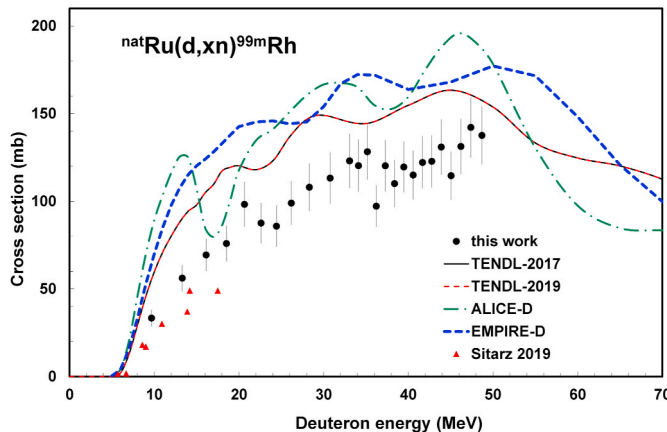


Fig. 8. Experimental excitation function of the $^{nat}\text{Ru}(d,xn)^{99m}\text{Rh}$ reaction in comparison with theoretical results.

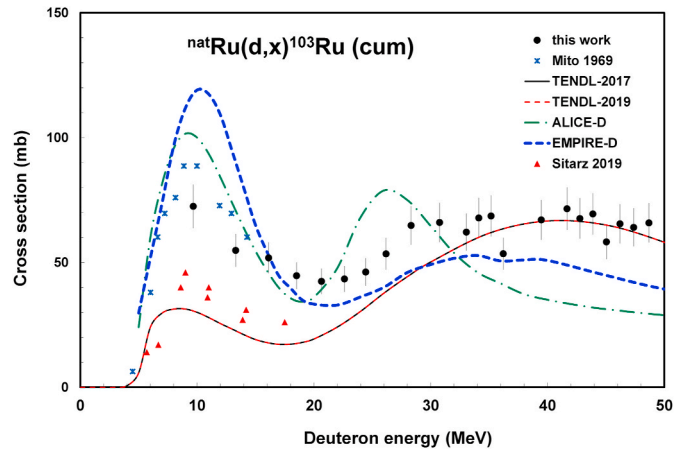


Fig. 11. Experimental excitation functions of the $^{nat}\text{Ru}(d,x)^{103}\text{Ru}$ reaction in comparison with literature values and theoretical results.

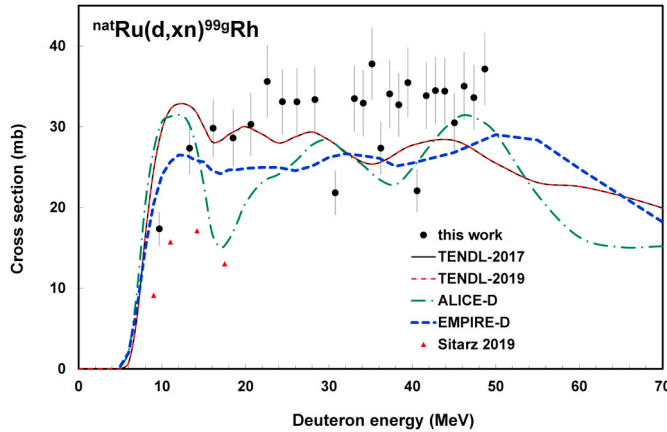


Fig. 9. Experimental excitation function of the $^{nat}\text{Ru}(d,xn)^{99g}\text{Rh}$ reaction in comparison with theoretical results.

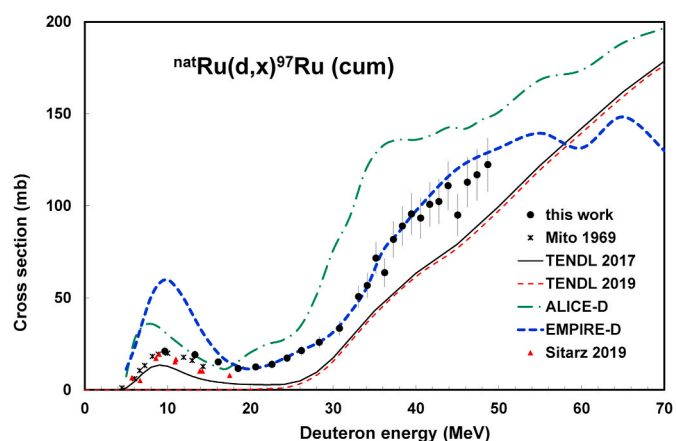


Fig. 12. Experimental excitation functions of the $^{nat}\text{Ru}(d,x)^{97}\text{Ru}$ reaction in comparison with literature values and theoretical results.

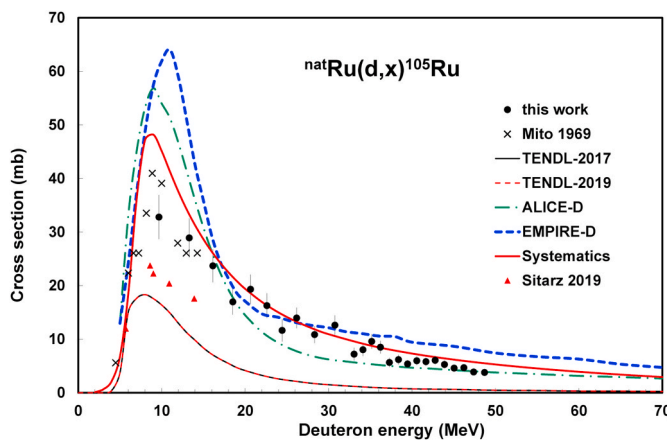


Fig. 10. Experimental excitation functions of the $^{nat}\text{Ru}(d,x)^{105}\text{Ru}$ reaction in comparison with literature values and theoretical results.

the TENDL versions underestimate the experimental results in the whole energy region. The low energy experimental literature data of (Sitarz, 2019) are lower than ours.

4.2.2. The $^{nat}\text{Ru}(d,x)^{103}\text{Ru}$ process

The ^{103}Rh ($T_{1/2} = 39.247$ d, IT: 100%) is produced directly and

through the decay of short-lived ^{103}Tc (54.2 s, β^- : 100%). The measured cumulative cross sections, the normalized (d,p) literature data (Mito et al., 1969; Sitarz, 2019) and the theoretical results are shown in Fig. 11. The low energy data of (Mito et al., 1969) are 20% higher than our data and the data of (Sitarz, 2019) are much lower than our values at the same energy. The theoretical codes agreements are varying: above

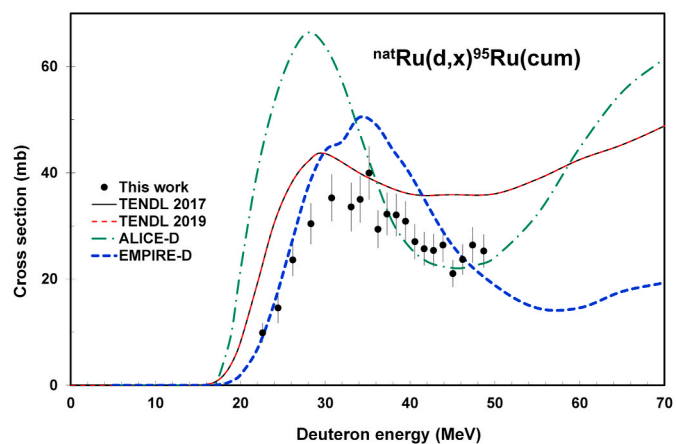


Fig. 13. Experimental excitation function of the $^{nat}\text{Ru}(d,x)^{95}\text{Ru}$ reaction in comparison with theoretical results.

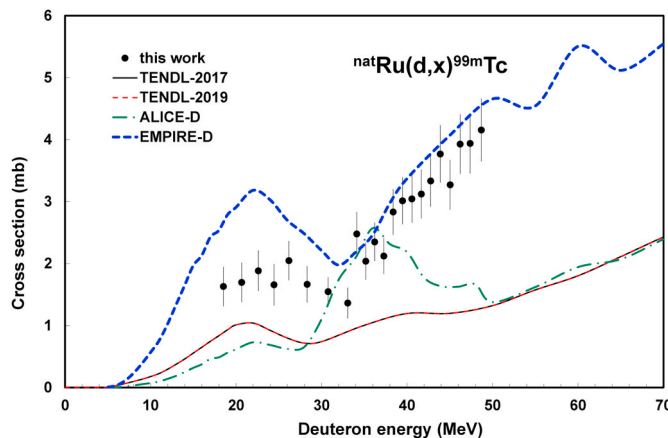


Fig. 14. Experimental excitation function of the $^{nat}\text{Ru}(d,x)^{99m}\text{Tc}$ reaction in comparison with theoretical results.

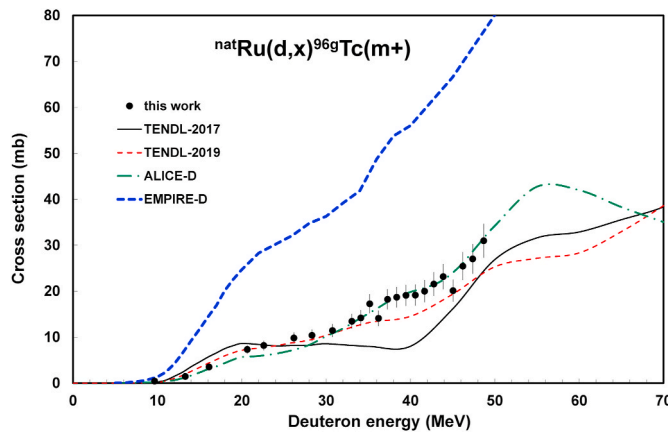


Fig. 15. Experimental excitation function of the $^{nat}\text{Ru}(d,x)^{96g}\text{Tc}$ reaction in comparison with theoretical results.

30 MeV the TENDL, below it the EMPIRE-D down to 15 MeV and below 15 MeV the ALICE-D, with a little overestimation, are acceptable. The TENDL predictions underestimate strongly below 30 MeV.

4.2.3. The $^{nat}\text{Ru}(d,x)^{97}\text{Ru}$ process

The experimental results for production of the ^{97}Ru ($T_{1/2} = 2.83$ d, $\varepsilon: 100\%$) (Fig. 12) include the total decay of ^{97m}Rh ($T_{1/2} = 46.2$ min, IT: 5.6%, $\varepsilon: 94.4\%$) and ^{97g}Rh (30.7 min, $\varepsilon: 100\%$). In principle the ^{97m}Tc ($T_{1/2} = 91.0$ d, $\varepsilon: 3.94\%$, IT: 96.06%) and ^{97g}Tc decay ($T_{1/2} = 4.21 \times 10^{-6}$ y, $\varepsilon: 100\%$) also contribute to the formation, but due to the significantly longer half-life it can be neglected under the present experimental conditions. In Fig. 12 the experimental data of (Mito et al., 1969; Sitarz, 2019) for $^{96}\text{Ru}(d,p)^{97}\text{Ru}$ reaction (normalized to ^{nat}Ru composition) and the theoretical predictions are also presented. The EMPIRE-D gives an excellent estimation above 18 MeV, between 10 and 18 MeV ALICE D is better. The TENDL results underestimate in the whole energy region and a small difference can be seen between the 2017 and 2019 versions.

4.2.4. The $^{nat}\text{Ru}(d,x)^{95}\text{Ru}$ process

The measured cross sections for production of ^{95}Ru ($T_{1/2} = 1.643$ h, $\varepsilon: 100\%$) (Fig. 13) are cumulative as they contain the contribution of the decay of the ^{95m}Rh ($T_{1/2} = 1.96$ min, IT: 88%, $\varepsilon: 12\%$) and ^{95g}Rh ($T_{1/2} = 5.02$ min, $\varepsilon: 100\%$) parents (Fig. 13). The EMPIRE-D approximation is acceptable up to 18 MeV, while between 35 and 50 MeV the ALICE-D estimation is better.

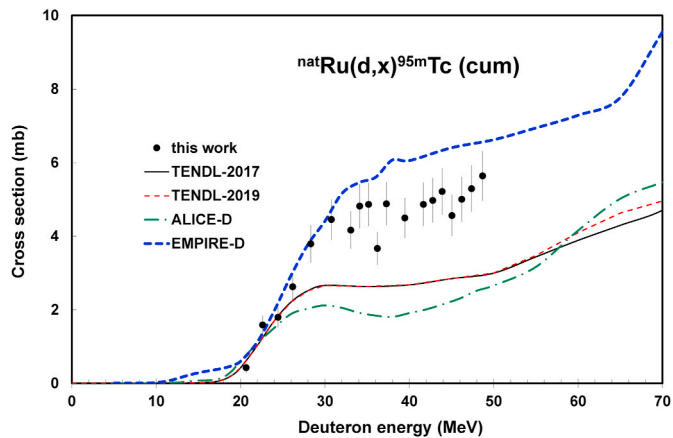


Fig. 16. Experimental excitation function of the $^{nat}\text{Ru}(d,x)^{95m}\text{Tc}$ reaction in comparison with theoretical results.

4.3. Cross sections of residual radionuclides of technetium

The radioisotopes of technetium are produced by direct ($d, 2pxn$) reactions (possibly clustered into α -emission) and through the decay of parent ruthenium radioisotopes. The contributing reactions and the reaction Q-values are presented in Table 2.

4.3.1. The $^{nat}\text{Ru}(d,x)^{99m}\text{Tc}$ process

We have obtained cross sections for direct ($d, 2pxn$) production of the ^{99m}Tc isomeric state ($T_{1/2} = 6.0072$ h, $\beta^-: 0.0037\%$, IT: 99.9963%) (Fig. 14). Due to the very long half-life of ^{99g}Tc ($T_{1/2} = 2.111 \times 10^5$ y, $\beta^-: 100\%$) it is practically impossible that any significant amount is contributed by the mother decay. EMPIRE gives a good approximation above 32 MeV but overestimates the peak around 22 MeV. All other theoretical models fail in a great amount.

4.3.2. The $^{nat}\text{Ru}(d,x)^{96g}\text{Tc}$ process

The ground state ^{96g}Tc ($T_{1/2} = 4.28$ d, $\varepsilon: 100\%$) is produced directly and by the decay of its short-lived isomeric state ^{96m}Tc ($T_{1/2} = 51.5$ min, $\varepsilon: 2.0\%$, IT: 98%). Due to the several hours of cooling time between EOB and the first spectra measurement the isomeric state practically decayed out and its activity was not detected. The cross sections of the ^{96g}Tc ($m+$) are shown in Fig. 15. The best prediction for the experimental results is given by the ALICE-D in the whole energy region. The approximation of the TENDL-2019 is also acceptable, and in this figure the improvement from TENDL-2017 to 2019 is clearly seen.

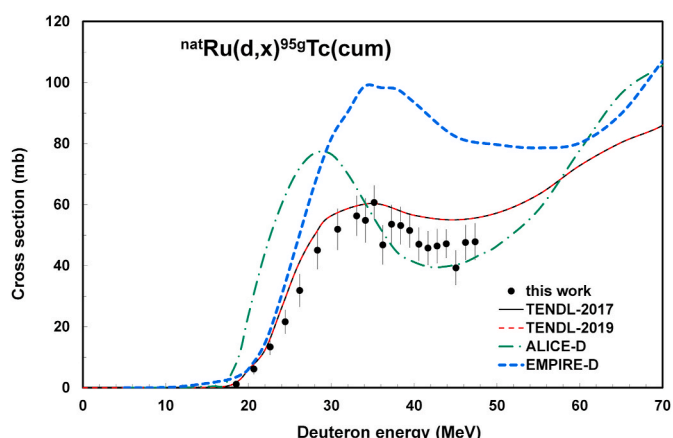


Fig. 17. Experimental excitation function of the $^{nat}\text{Ru}(d,x)^{95g}\text{Tc}$ reaction in comparison with theoretical results.

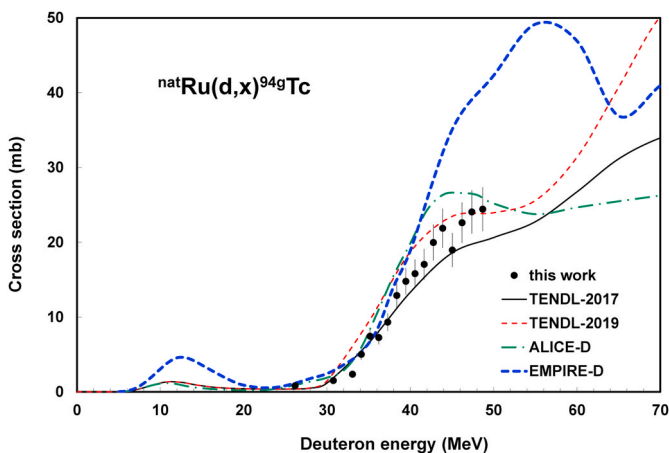


Fig. 18. Experimental excitation function of the $^{nat}\text{Ru}(d,x)^{94g}\text{Tc}$ reaction in comparison with theoretical results.

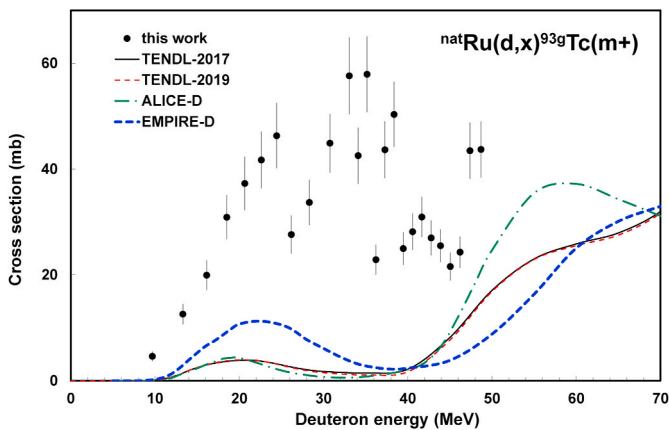


Fig. 19. Experimental excitation function of the $^{nat}\text{Ru}(d,x)^{93g}\text{Tc}$ reaction in comparison with theoretical results.

4.3.3. The $^{nat}\text{Ru}(d,x)^{95m}\text{Tc}$ process

The radionuclide ^{95}Tc has two isomeric states: a longer-lived metastable state ^{95m}Tc ($T_{1/2} = 61$ d, $\varepsilon: 96.12\%$, IT: 3.88%) and the ground state ^{95g}Tc ($T_{1/2} = 20.0$ h, $\varepsilon: 100\%$). Both states are populated by decay of the ^{95}Ru ($T_{1/2} = 1.643$ h, $\varepsilon: 100\%$) parent. The cross section data of ^{95m}Tc represent cumulative cross sections, obtained from spectra measured after the complete decay of ^{95}Ru parent (Fig. 16). The estimation of the EMPIRE-D is the best again, ALICE-D and both TENDL versions underestimate above 25 MeV.

4.3.4. The $^{nat}\text{Ru}(d,x)^{95g}\text{Tc}$ process

The cumulative cross section data for ^{95g}Tc ($T_{1/2} = 20.0$ h) were deduced from the second series of spectra measurements (21.7–29.0 h) after EOB, where ^{95}Ru ($T_{1/2} = 1.643$ h) decayed out and the contribution of the decay of longer-lived ^{95m}Tc ($T_{1/2} = 61$ d, $\varepsilon: 96.12\%$, IT: 3.88%) can be practically neglected according to our calculation. The measured ^{95g}Tc cross sections hence represent the direct production plus the decay of ^{95}Ru (Fig. 17). In this case the approximation of the TENDL versions is acceptable.

4.3.5. The $^{nat}\text{Ru}(d,x)^{94g}\text{Tc}$ process

Out of the two listed isomers of ^{94}Tc we can deduce cross sections only for production of the ground state ^{94g}Tc ($T_{1/2} = 293$ min, $\varepsilon: 100\%$), as the rather short half-life of the metastable ^{94m}Tc ($T_{1/2} = 52.0$ min, $\varepsilon: 100\%$) and the time schedule of our gamma spectra measurement did not allow assessment of its activity. The measured cross sections are cumulative containing the complete decay of ^{94}Ru ($T_{1/2} = 51.8$ min, $\varepsilon: 100\%$) (Fig. 18). In this case the approximations of the 4 model codes/versions run together from 20 to 40 MeV and show also acceptable agreement with our new results. Above 40 MeV the TENDL-2019 estimation gives acceptable results.

4.3.6. The $^{nat}\text{Ru}(d,x)^{93g}\text{Tc}$ process

The ^{93g}Tc (2.75 h, $\varepsilon: 100\%$) is produced directly, from the decay of its isomeric state (^{93m}Tc , 43.5 min, $\varepsilon: 22.6\%$, IT: 77.4%) and through the decay of the ^{93m}Ru (10.8 s, IT: 22.0%, $\varepsilon: 78\%$) and ^{93g}Ru (59.7 s, $\varepsilon: 100\%$) parent isotopes. The measured and calculated cross sections are shown in Fig. 19. The experimental data have large uncertainties, due to the low statistics and it can be a reason why the comparison with the theoretical model calculations only shows a general underestimation of the experimental results.

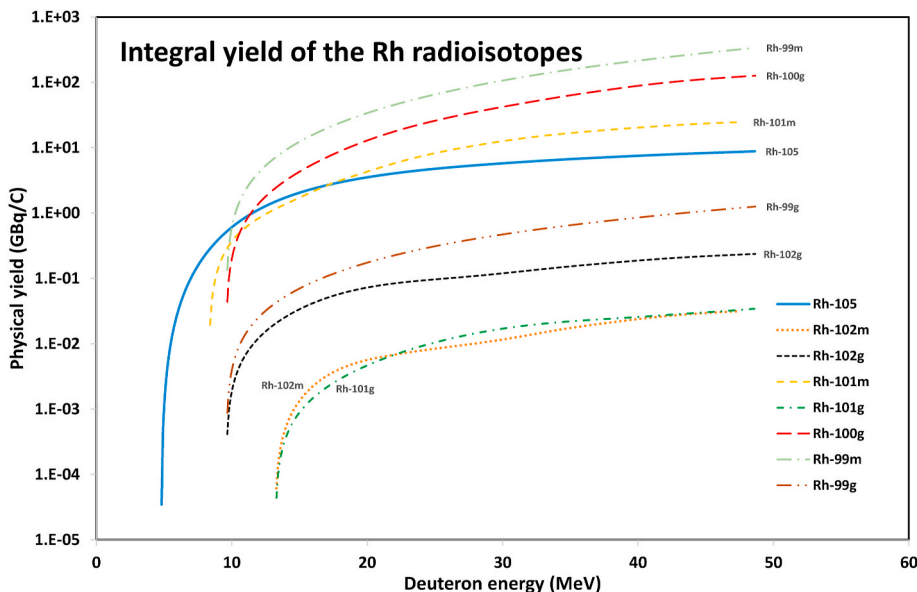


Fig. 20. Integral thick target yields for the formation of the investigated radioisotopes of rhodium as a function of the energy.

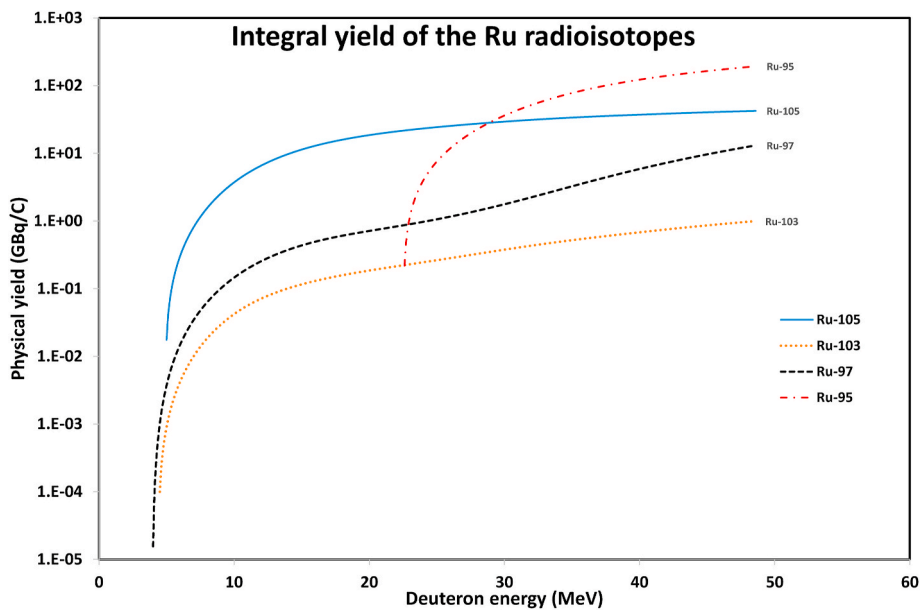


Fig. 21. Integral thick target yields for the formation of the investigated radioisotopes of ruthenium as a function of the energy.

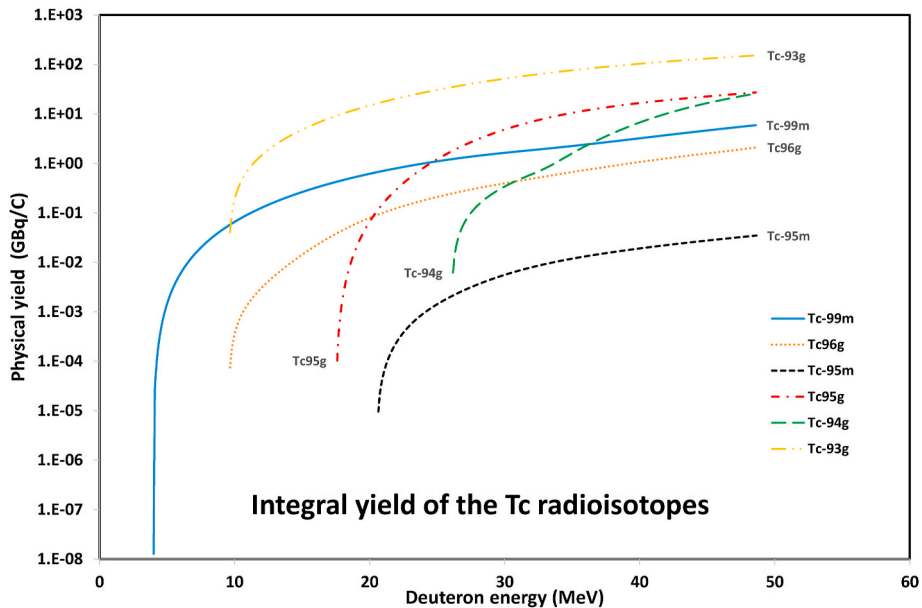


Fig. 22. Integral thick target yields for the formation of the investigated radioisotopes of technetium as a function of the energy.

5. Integral yields

The integral yields calculated from spline fits to our experimental excitation functions are shown in Figs. 20–22. The integral yields represent so called physical yields i.e. activity for instantaneous production rates (Bonardi, 1987; Otuka and Takacs, 2015). No experimental thick target yield data were found in the literature for comparison.

6. On application for production of medical radioisotopes

We shortly summarize the possible role of the deuteron induced reactions on ruthenium for production of medical radioisotopes, by comparing integral production yields of charged particle production routes for ^{105}Rh , $^{103}\text{Ru}/^{103m}\text{Rh}$, ^{101}Rh , ^{101}Rh , ^{97}Ru , ^{99m}Tc and ^{95g}Tc . In practice of course also many other factors play an important role in the

selection of an optimal production route (available accelerator, radionuclide purity and specific activity, target preparation and recovery, required chemical separation, etc.). We compare the production yield on natural targets as deduced from cross section results of our group or from the activation database, if a reaction was not studied by us, with the aim to indicate the production power of deuterons. For real production of medical isotopes, the comparison has to be more specific as often using nuclear reactions on highly enriched monoisotopic targets is required, especially to ensure better purity and specific activity of the end product.

6.1. Production of ^{105}Rh

The radionuclide ^{105}Rh is considered as a low-energy β^- emitter for therapy in small tumors. ^{105}Rh radionuclide can be produced by nuclear reactors using an enriched ^{104}Ru target via the indirect $^{104}\text{Ru}(\text{n},\gamma)^{105}\text{Ru}$

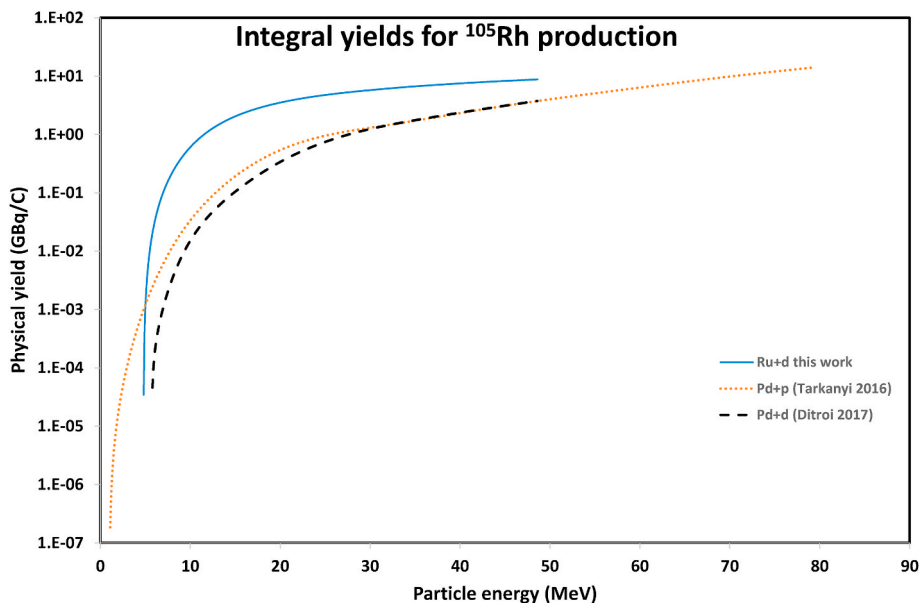


Fig. 23. Integral yields of charged particle induced reactions for production of ^{105}Rh .

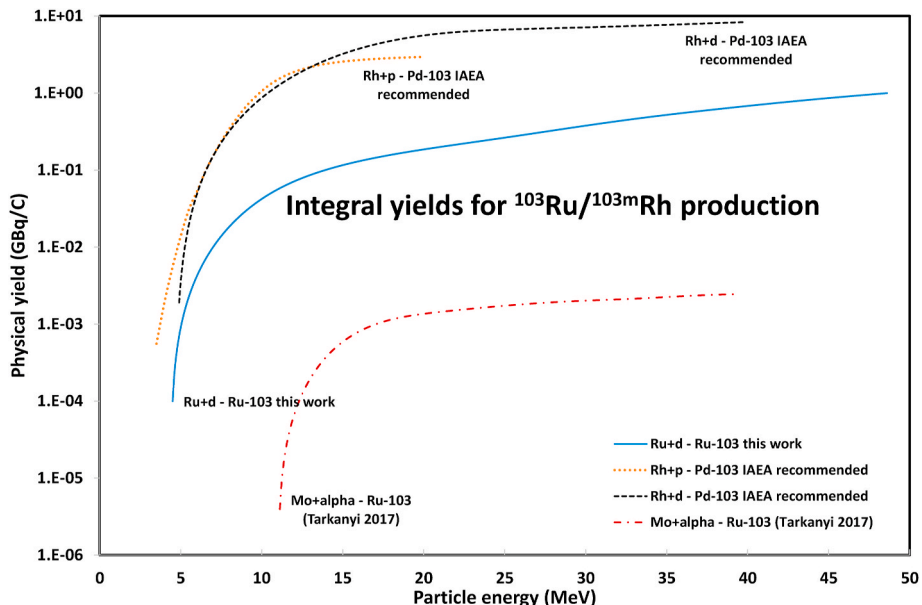


Fig. 24. Integral yields of charged particle induced reactions for production of $^{103}\text{Ru}/^{103\text{m}}\text{Rh}$.

$\rightarrow ^{105}\text{Rh}$ processes. It is also possible to obtain ^{105}Rh as a fission product of uranium and thorium.

^{105}Rh can also be produced using cyclotrons through the proton and deuteron irradiations on palladium targets or deuteron induced reactions on ruthenium. The corresponding integral yields for charged particle routes are shown in Fig. 23. The integral yields are based on experimental cross sections Tarkanyi 2016 (Tarkányi et al., 2016) for ${}^{\text{nat}}\text{Pd}(\text{p},\text{x})^{105}\text{Rh}$ and of (Ditrói et al., 2012a) and (Ditrói et al., 2017) for ${}^{\text{nat}}\text{Pd}(\text{d},\text{x})^{105}\text{Rh}$ and our present data for ${}^{\text{nat}}\text{Ru}(\text{d},\text{xn})^{105}\text{Rh}$ reaction. Additional cross section data from r (Khandaker et al., 2010) also exist but were not exploited here. From Fig. 23 it is obvious that the highest yield can be reached by irradiation of ruthenium targets with deuterons. Even the energy range is within the deuteron energy of the compact cyclotrons. The proton and deuteron reactions on Pd have lower, but very similar yields.

6.2. Production of $^{103}\text{Ru}/^{103\text{m}}\text{Rh}$

^{103}Pd is a parent isotope (EC decay) of $^{103\text{m}}\text{Rh}$ ($T_{1/2} = 56.1$ min), an isotope of interest for Auger electron therapy. The integral yield data for production of ^{103}Pd using proton or deuteron induced reactions on ^{103}Rh via the $^{103}\text{Rh}(\text{p},\text{n})^{103}\text{Pd}$ and $^{103}\text{Rh}(\text{d},2\text{n})^{103}\text{Pd}$ reactions were taken from the IAEA recommended database (Qaim et al., 2011).

Another route to produce $^{103\text{m}}\text{Rh}$ is the β^- decay of parent ^{103}Ru ($T_{1/2} = 39.35$ d). The ^{103}Ru can be obtained as fission products of ^{235}U (n, f) ^{103}Ru or ^{232}Th (p, f) ^{103}Ru (not exploited here), by alpha induced reactions on molybdenum ((Graf and Munzel, 1974), (Esterlund and Pate, 1965), (Abe et al., 1984), (Ditrói et al., 2012b) and (Tarkanyi et al., 2017)) and via proton (in progress) and deuteron induced reactions (this work) on ruthenium. The integral yields deduced from cross section measurements of our group ([26] and this work) are shown in Fig. 24. For production of $^{103\text{m}}\text{Rh}$ the proton and deuteron induced reactions on

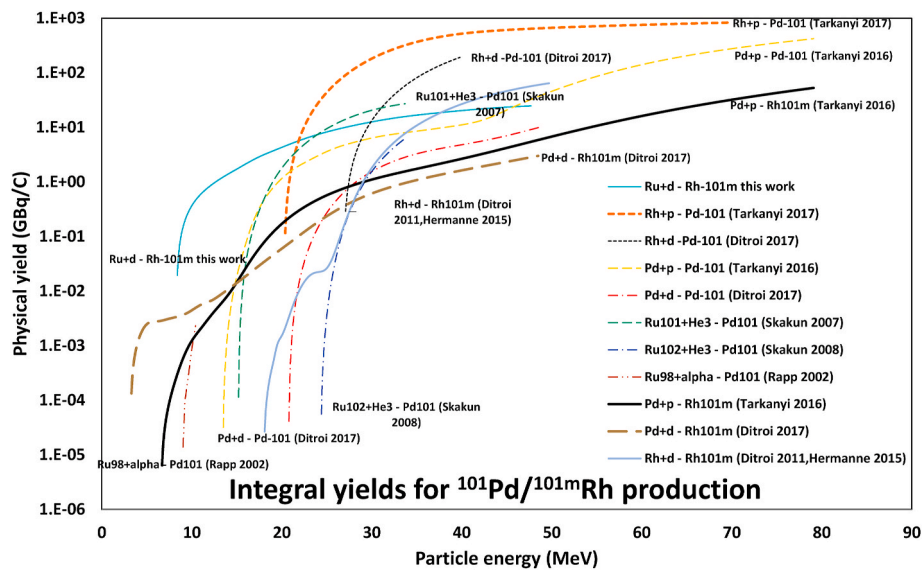


Fig. 25. Integral yields of charged particle induced reactions for production of ^{101}mRh .

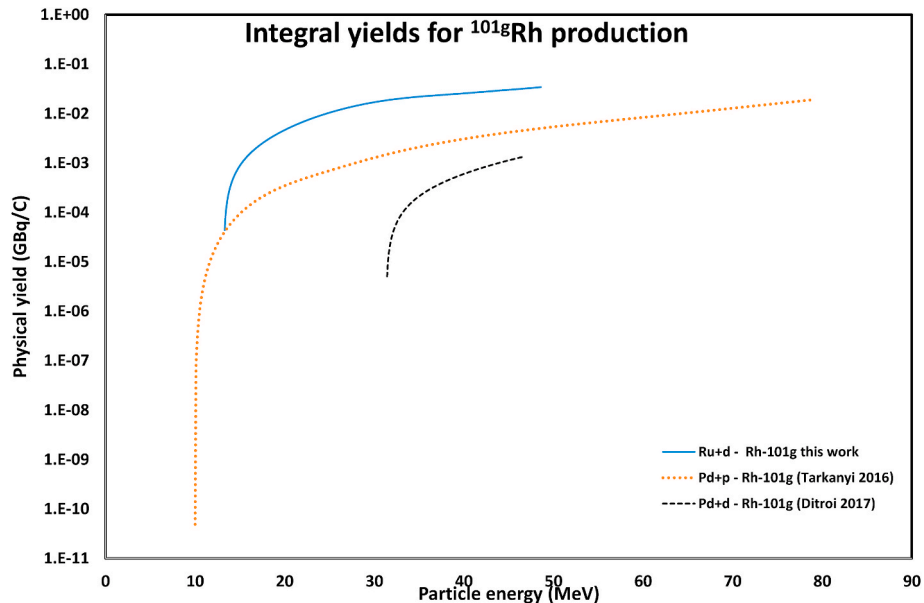


Fig. 26. Integral yields of charged particle induced reactions for production of ^{101}gRh .

^{103}Rh (through parent ^{103}Pd) are the favorites. All the routes through ^{103}Ru mother are less productive.

6.3. Production of ^{101}mRh

^{101}mRh ($T_{1/2} = 4.4$ d) is a potential candidate for targeted radiotherapeutic use due to its nuclear decay and chemical properties. The ^{101}mRh can be produced indirectly through EC decay of its shorter-lived ^{101}Pd parent. Cross sections for formation of ^{101}Pd were investigated by several routes: via $^{103}\text{Rh(p,3n)}^{101}\text{Pd}$ ((Lagunassolar et al., 1984), (Hermann et al., 2000), (Tárkányi et al., 2017), (Sudar et al., 2002)), $^{103}\text{Rh(d,4n)}^{101}\text{Pd}$ (Ditrói et al., 2011), (Hermann et al., 2015), $^{\text{nat}}\text{Pd(p,x)}^{101}\text{Pd}$ (Khandaker et al., 2010) (Tárkányi et al., 2016)), $^{\text{nat}}\text{Pd(d,x)}^{101}\text{Pd}$ (Ditrói et al., 2012a), (Ditrói et al., 2017)), $^{101}\text{Ru}({}^3\text{He},x)^{101}\text{Pd}$ ((Skakun and Qaim, 2007), $^{102}\text{Ru}({}^3\text{He},x)^{101}\text{Pd}$ (Skakun and Qaim, 2008)), $^{98}\text{Ru}(\alpha,n)^{101}\text{Pd}$ ((Rapp et al., 2001), (Rapp et al., 2002)) or directly $^{\text{nat}}\text{Pd(p,x)}^{101}\text{mRh}$ (Ditrói et al., 2007), (Khandaker et al.,

2010), (Tárkányi et al., 2016), (Hien et al., 2018)), $^{\text{nat}}\text{Pd(d,x)}^{101}\text{mRh}$ ((Ditrói et al., 2012a), (Ditrói et al., 2017)), $^{103}\text{Rh(d,x)}^{101}\text{mRh}$ (Ditrói et al., 2011; Hermann et al., 2015; Manenti et al., 2017), $^{\text{nat}}\text{Ru(p,x)}^{101}\text{mRh}$ or $^{\text{nat}}\text{Ru(d,x)}^{101}\text{mRh}$ (this work) reactions. The integral yields deduced from selected datasets (mostly our group) are collected in Fig. 25. According to Fig. 25 the proton and deuteron induced reactions on Rh (monoisotopic ^{103}Rh) are the favorites. Indirect process through ^{101}Pd parent is the most efficient at energies above 20–25 MeV, but under 10 MeV, the energy range of the small compact cyclotrons with deuteron option the Ru + d and Pd + d reaction producing ^{101}mRh directly can give attractive yields.

6.4. Production of ^{101}gRh

Long-lived ^{101}gRh ($T_{1/2} = 3.3$ y) is proposed as an alternative to the existing High Dose Rate sources used in brachytherapy. This radionuclide can be produced indirectly through ^{101}Pd (see ^{101}mRh above) and

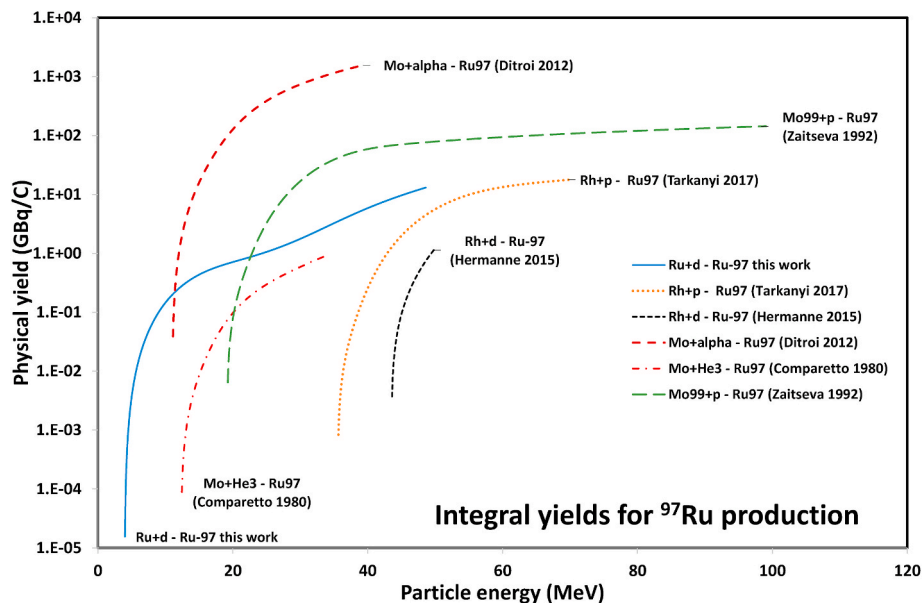


Fig. 27. Integral yields of charged particle induced reactions for production of ^{97}Ru .

directly via $^{\text{nat}}\text{Pd}(\text{p},\text{x})^{101}\text{gRh}$ ((Tárkányi et al., 2016), (Hien et al., 2018)), $^{\text{nat}}\text{Pd}(\text{d},\text{x})^{101}\text{gRh}$ ((Ditroi et al., 2012a), (Ditroi et al., 2017)), $^{\text{nat}}\text{Ru}(\text{d},\text{x})^{101}\text{gRh}$ (this work). Integral yields of charged particle induced reactions, based on results of our group, are collected in Fig. 26. The deuteron induced reaction on Ru has the highest yields for production of ^{101}gRh (Fig. 26).

6.5. Production of ^{97}Ru

The radionuclide ^{97}Ru emits low-energy high-intensity gamma-lines with favorable characteristics for Single Photon Emission Computed Tomography (SPECT) examinations. It forms a theranostic matched pair with ^{103}Ru ($T_{1/2} = 39.26$ d) that decays to the short-lived Auger emitter ^{103m}Rh ($T_{1/2} = 56.12$ min). Accelerator methods to produce ^{97}Ru found in the literature are: $^{103}\text{Rh}(\text{p},\text{x})^{97}\text{Ru}$ (essentially $(\text{p},\alpha 3n)$ above 22 MeV proton energy) ((Lagunassolar et al., 1983), (Tárkányi et al., 2017)), $^{103}\text{Rh}(\text{d},\text{x})^{97}\text{Ru}$ ((Hermann et al., 2015)), $^{\text{nat}}\text{Mo}(\alpha,\text{xn})^{97}\text{Ru}$ ((Ditroi

et al., 2012b), (Tarkanyi et al., 2017), (Sitarz et al., 2019)), (Comparetto and Qaim, 1980)), $^{94}\text{Mo}(\alpha,\text{x})^{97}\text{Ru}$ ((Rapp et al., 2008), (Graf and Munzel, 1974)), $^{95}\text{Mo}(\alpha,\text{x})^{97}\text{Ru}$ (Levkovskii, 1991), $^{96}\text{Mo}(\alpha,\text{x})^{97}\text{Ru}$ ((Levkovskii, 1991), $^{\text{nat}}\text{Mo}(\text{He},\text{xn})^{97}\text{Ru}$ (Comparetto and Qaim, 1980), $^{99}\text{Tc}(\text{p},\text{3n})^{97}\text{Ru}$ (Zaitseva et al., 1992), $^{\text{nat}}\text{Ru}(\text{d},\text{x})^{97}\text{Ru}$ this work. Some calculated yields are presented in Fig. 27. The highest yield can be reached with the Mo+ α reaction using a rather cheap natural Mo target. The yield should be much higher, but targets more expensive and need recovery, by using any of the stable Mo isotopes in enriched form. Taking into account that the alpha option is not common for a compact cyclotron, the Ru + d reaction, presented here, can be competitive (Fig. 27).

6.6. Production of ^{99m}Tc

Technetium-99 m is the worldwide most used radioactive tracer for SPECT. It can be produced directly or through the decay of its ^{99}Mo

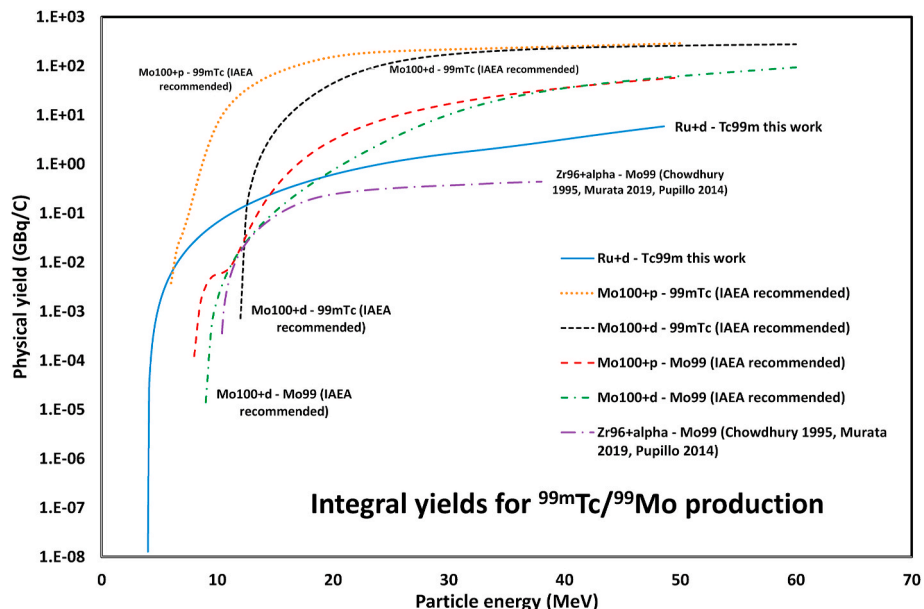


Fig. 28. Integral yields of charged particle induced reactions for production of ^{99m}Tc .

parent. Direct production charged particle routes include: ^{100}Mo ($\text{p},\text{2n}$) ^{99m}Tc ((Manenti et al., 2014; Tarkanyi et al., 2019), $^{100}\text{Mo}(\text{d},\text{3n})$ ^{99m}Tc (Tarkanyi et al., 2019), $^{\text{nat}}\text{Ru}(\text{d},\text{x})$ ^{99m}Tc (this work), $^{\text{nat}}\text{Ru}$ (p,x) ^{99m}Tc ((Gagnon et al., 2017), our group in progress). The commercially most important indirect production routes is through ^{99}Mo decay based on reactor neutron reactions: $\text{U}(\text{n},\text{f})$ ^{99}Mo . Alternative charged particle induced routes are: $^{100}\text{Mo}(\text{p},\text{pn})$ ^{99}Mo (Manenti et al., 2014; Tarkanyi et al., 2019), $^{100}\text{Mo}(\text{d},\text{p2n})$ ^{99}Mo (Tarkanyi et al., 2019), $^{96}\text{Zr}(\alpha,\text{n})$ ^{99}Mo ((Chowdhury et al., 1995), (Murata et al., 2019), (Pupillo et al., 2014)) as well as the reactor based neutron reaction: ^{98}Mo (n,γ) ^{99}Mo . The comparison in Fig. 28 shows that for production of ^{99m}Tc the proton and deuteron induced reactions on ^{100}Mo are the favorites.

7. Summary and conclusions

We have measured the excitation functions on natural ruthenium for production of ^{105}Rh , ^{102m}Rh , ^{102g}Rh , ^{101m}Rh , ^{101g}Rh , ^{100g}Rh , ^{99m}Rh , ^{99g}Rh , ^{105}Ru , ^{103}Ru (cum), ^{102}Ru (cum), ^{97}Ru (cum), ^{95}Ru (cum), ^{99m}Tc , ^{96g}Tc (m+), ^{95m}Tc (cum), ^{95g}Tc (cum), ^{94g}Tc , ^{93g}Tc (m+) up to 50 MeV and presented cross section results for the first time in the whole energy range. The experimental cross sections are compared with our calculations using the ALICE-D and EMPIRE-D theoretical codes and with TALYS (from TENDL database) theoretical results, showing in many cases significant disagreements.

In several of our earlier studies we have shown that deuteron induced reactions are competitive with protons, especially for targets above the middle mass region. This opens also the possibility to produce additional products, not reachable with proton reactions on the same targets, by using (d,n), and (d,p) reactions. For production of isotopes the widely used H^+ cyclotrons can, if the option is foreseen, also assure high intensity deuteron beams. To illustrate the production power of deuteron induced reactions we have compared the production yields of the presently studied reactions with other light charged particles for production of a few medical isotopes. The comparison shows that the deuteron induced nuclear reactions, from point of view the production yields, are in many cases promising.

Declaration of competing interest

The authors declare that they have no known competing financial interests or personal relationships that could have appeared to influence the work reported in this paper.

Acknowledgement

The authors acknowledge the support of the respective institutions and the accelerator staffs for providing the beam time and experimental facilities.

References

- Abe, K., Iizuka, A., Hasegawa, A., Morozumi, S., 1984. Induced radioactivity of component materials by 16-mev protons and 30-mev alpha-particles. *J. Nucl. Mater.* 123, 972–976.
- Andersen, H.H., Ziegler, J.F., 1977. Hydrogen Stopping Powers and Ranges in All Elements. The Stopping and Ranges of Ions in Matter, vol. 3. Pergamon Press, New York.
- Bonardi, M., 1987. The contribution to nuclear data for biomedical radioisotope production from the Milan cyclotron facility. In: Okamoto, K. (Ed.), Consultants Meeting on Data Requirements for Medical Radioisotope Production. IAEA, INDC (NDS)-195 (1988), Tokyo, Japan, pp. 98–112.
- Canberra, 2000. http://www.canberra.com/products/radiochemistry_lab/genie-2000-software.asp.
- Chowdhury, D.P., Pal, S., Saha, S.K., Gangadharan, S., 1995. Determination of cross-section of alpha-induced nuclear-reaction on natural Cr and Zr by stacked foil activation for thin-layer activation-analysis. *Nucl. Instrum. Methods Phys. Res., Sect. B* 103, 261–266.
- Comparetto, G., Qaim, S.M., 1980. A comparative-study of the production of short-lived neutron deficient isotopes Ru-94,95,97 in alpha-particle and He-3-Particle induced nuclear-reactions on natural molybdenum. *Radiochim. Acta* 27, 177–180.
- Ditrói, F., Tárkányi, F., Takács, S., Mahunka, I., Csikai, J., Hermanne, A., Uddin, M.S., Hagiwara, M., Baba, M., Ido, T., Shubin, Y., Dityuk, A.I., 2007. Measurement of activation cross sections of the proton induced nuclear reactions on palladium. *J. Radioanal. Nucl. Chem.* 272, 231–235.
- Ditrói, F., Tárkányi, F., Takács, S., Hermanne, A., Yamazaki, H., Baba, M., Mohammadi, A., Ignatyuk, A.V., 2011. Study of activation cross-sections of deuteron induced reactions on rhodium up to 40 MeV. *Nucl. Instrum. Methods Phys. Res., Sect. B* 269, 1963–1972.
- Ditrói, F., Tárkányi, F., Takács, S., Hermanne, A., Ignatyuk, A.V., Baba, M., 2012a. Activation cross-sections of deuteron induced reactions on natural palladium. *Nucl. Instrum. Methods Phys. Res., Sect. B* 270, 61–74.
- Ditrói, F., Hermanne, A., Tárkányi, F., Takács, S., Ignatyuk, A.V., 2012b. Investigation of the α -particle induced nuclear reactions on natural molybdenum. *Nucl. Instrum. Methods Phys. Res., Sect. B* 285, 125–141.
- Ditrói, F., Tárkányi, F., Takács, S., Hermanne, A., Ignatyuk, A.V., Baba, M., 2012c. Activation cross-sections of deuteron induced reactions on natural palladium. *Nucl. Instrum. Methods Phys. Res., Sect. B* 270, 297–306.
- Dityuk, A.I., Konobeyev, A.Y., Lunev, V.P., Shubin, Y.N., 1998. New Version of the Advanced Computer Code ALICE-IPPE, INDC (CCP)-410. IAEA, Vienna.
- Esterlund, E.A., Pate, B.D., 1965. Analysis of excitation functions via the compound statistical model. *Nucl. Phys.* 69, 401.
- Gagnon, K., Wilson, J.S., Holt, C.M.B., Lapi, S.E., Ferguson, S., Mitlin, D., McQuarrier, S.A., 2017. Excitation functions for proton-induced reactions on $^{\text{nat}}\text{Ru}$ from 7 to 18 MeV. *J. of Labelled Compounds and Radiopharmaceut* 60, S324.
- Graf, H.P., Munzel, H., 1974. Excitation functions for α -particle reactions with molybdenum isotopes. *J. Inorg. Nucl. Chem.* 36, 3647.
- Herman, M., Capote, R., Carlson, B.V., Oblozinsky, P., Sin, M., Trkov, A., Wienke, H., Zerkin, V., 2007. EMPIRE: nuclear reaction model code system for data evaluation. *Nucl. Data Sheets* 108, 2655–2715.
- Hermann, A., Sonck, M., Fenyesi, A., Darabani, L., 2000. Study on production of ^{103}Pd and characterisation of possible contaminants in the proton irradiation of ^{103}Rh up to 28 MeV. *Nucl. Instrum. Methods Phys. Res., Sect. B* 170, 281–292.
- Hermann, A., Tárkányi, F., Takacs, S., Ditrói, F., 2015. Extension of activation cross section data of deuteron induced nuclear reactions on rhodium up to 50 MeV. *Nucl. Instrum. Methods Phys. Res., Sect. B* 362, 110–115.
- Hien, N.T., Van Do, N., Luan, N.T., Kim, G., Kim, K., Uddin, M.S., Naik, H., 2018. Excitation functions and cross section ratios for the formation of the isomeric pairs Rh-102m,Rh-g;101m,Rh-g;99m,Rh-g in the Pd-nat(p,2px) reactions. *Nucl. Instrum. Methods Phys. Res., Sect. B* 429, 1–8.
- International-Bureau-of-Weights-and-Measures, 1993. Guide to the Expression of Uncertainty in Measurement, first ed. International Organization for Standardization, Genève, Switzerland.
- Khandaker, M.U., Kim, K., Kim, G., Otuka, N., 2010. Cyclotron production of the Ag-105, Ag-106m, Pd-100,Pd-101, Rh-100,Rh-101m,Rh-105 radionuclides by Pd-nat(p,x) nuclear processes. *Nucl. Instrum. Methods Phys. Res., Sect. B* 268, 2303–2311.
- Koning, A.J., Rochman, D., 2012. Modern nuclear data evaluation with the TALYS code system. *Nucl. Data Sheets* 113, 2841–3172.
- Koning, A.J., Rochman, D., Sublet, J.C., 2017. TENDL-2017 TALYS-based evaluated nuclear data library. https://tendl.web.psi.ch/tendl_2017/tendl2017.html.
- Koning, A.J., Rochman, D., Sublet, J.C., Dzysiuk, N., Fleming, M., van der Marck, S., 2019. TENDL-2019. https://tendl.web.psi.ch/tendl_2019/tendl2019.html.
- Laboratory, B.N., 2019. Nudat 2.8. <https://www.ndc.bnl.gov/nudat2/>.
- Lagunassolar, M.C., Avila, M.J., Navarro, N.J., Johnson, P.C., 1983. Cyclotron production of No-Carrier-Added Ru-97 by proton-bombardment of Rh-103 targets. *Appl. Radiat. Isot.* 34, 915–922.
- Lagunassolar, M.C., Avila, M.J., Johnson, P.C., 1984. Cyclotron production of Rh-101m via proton-induced reactions on Rh-103 targets. *Appl. Radiat. Isot.* 35, 743–748.
- Levkovskii, V.N., 1991. The Cross-Sections of Activation of Nuclides of Middle-Range Mass (A=40-100) by Protons and Alpha Particles of Middle Range Energies (E=10-50 MeV). Inter-Vesyl, Moscow.
- Manenti, S., Holzwarth, U., Loriggiola, M., Gini, L., Esposito, J., Groppi, F., Simonelli, F., 2014. The excitation functions of Mo-100(p,x) Mo-99 and Mo-100(p,2n)Tc-99m. *Appl. Radiat. Isot.* 94, 344–348.
- Manenti, S., Santoro, M.D.A., Cotogno, G., Duchemin, C., Haddad, F., Holzwarth, U., Groppi, F., 2017. Excitation function and yield for the Rh-103(d,2n) Pd-103 nuclear reaction: optimization of the production of palladium-103. *Nucl. Med. Biol.* 49, 30–37.
- Mito, A., Komura, K., Mitsugashira, T., Otozai, K., 1969. Excitation functions for the (d,p) reactions on ^{96}Ru , ^{102}Ru and ^{104}Ru . *Nucl. Phys.* 129, 165–171.
- Murata, T., Aikawa, M., Saito, M., Ukon, N., Komori, Y., Haba, H., Takacs, S., 2019. Production cross sections of Mo, Nb and Zr radioisotopes from alpha-induced reaction on Zr-nat. *Appl. Radiat. Isot.* 144, 47–53.
- Otuka, N., Takacs, S., 2015. Definitions of radioisotope thick target yields. *Radiochim. Acta* 103, 1–6.
- Pritychenko, B., Sonzogni, A., 2003. Q-value Calculator. NNDC, Brookhaven National Laboratory. <http://www.ndc.bnl.gov/qcalc>.
- Pupillo, G., Esposito, J., Gambaccini, M., Haddad, F., Michel, N., 2014. Experimental cross section evaluation for innovative Mo-99 production via the (α ,n) reaction on Zr-96 target. *J. Radioanal. Nucl. Chem.* 302, 911–917.
- Qaim, S.M., Tárkányi, F., Capote, R., 2011. Nuclear Data for the Production of Therapeutic Radionuclides, Technical Reports Series 473. IAEA, Vienna, p. 1.
- Rapp, W., Brede, H.J., Heil, M., Hentschel, D., Käppeler, F., Klein, H., Reifarth, R., Rauscher, T., 2001. Alpha and neutron induced reactions on ruthenium. *Nucl. Phys.* 688, 427–429.

- Rapp, W., Heil, M., Hentschel, D., Kappeler, F., Reifarth, R., Brede, H.J., Klein, H., Rauscher, T., 2002. alpha- and neutron-induced reactions on ruthenium isotopes. Phys. Rev. C 66.
- Rapp, W., Dillmann, I., Kaeppeler, F., Giesen, U., Klein, H., Rauscher, T., Hentschel, D., Hilpp, S., 2008. Cross section measurements of alpha-induced reactions on (92,94) Mo and (112)Sn for p-process studies. Phys. Rev. C 78.
- Rosch, F., Qaim, S.M., Stocklin, G., 1993. Nuclear-data relevant to the production of the positron emitting radioisotope Y-86 via the Sr-86(P,N)-Processes and (nat)Rb(He-3, Xn)-Processes. Radiochim. Acta 61, 1–8.
- Sitarz, M., Nigrón, E., Guertin, A., Haddad, F., Matulewicz, T., 2019. New cross-sections for natMo(x,x) reactions and medical 97Ru production estimations with radionuclide yield calculator. Instruments 3, 7.
- Sitarz, M., 2019. Research on Production of New Medical Radioisotopes with Cyclotron. PhD thesis. niversité de Nantes, Nantes, France. <https://tel.archives-ouvertes.fr/tel-02458431>.
- Sakun, Y., Qaim, S.M., 2007. Excitation Functions of 3He-Particle Induced Reactions on 101Ru and 102Ru for Production of the Medically Interesting Radionuclide 101m Rh. Conf.on Nucl.Data for Sci. and Technology, Nice, France, p. 1379.
- Sakun, Y., Qaim, S.M., 2008. Measurement of excitation functions of helion-induced reactions on enriched Ru targets for production of medically important Pd-103 and Rh-101m and some other radionuclides. Appl. Radiat. Isot. 66, 653–667.
- Sudar, S., Cserpak, F., Qaim, S.M., 2002. Measurements and nuclear model calculations on proton-induced reactions on Rh-103 up to 40 MeV: evaluation of the excitation function of the Rh-103(p,n) Pd-103 reaction relevant to the production of the therapeutic radionuclide Pd-103. Appl. Radiat. Isot. 56, 821–831.
- Székely, G., 1985. Fgm - a flexible gamma-spectrum analysis program for a small computer. Comput. Phys. Commun. 34, 313–324.
- Tárkányi, F., Hermanne, A., Ditroi, F., Takács, S., Ignatyuk, A., 2017. Investigation of activation cross section data of alpha particle induced nuclear reaction on molybdenum up to 40 MeV: review of production routes of medically relevant Ru-97,Ru-103. Nucl. Instrum. Methods Phys. Res., Sect. B 399, 83–100.
- Tárkányi, F., Szelecsényi, F., Takács, S., 1991. Determination of effective bombardment energies and fluxes using improved stacked-foil technique. Acta Radiol. 376, 72. Suppl.
- Tárkányi, F., Takács, S., Gul, K., Hermanne, A., Mustafa, M.G., Nortier, M., Oblozinsky, P., Qaim, S.M., Scholten, B., Shubin, Y.N., Youxiang, Z., 2001. Beam Monitor Reactions (Chapter 4). Charged Particle Cross-Section Database for Medical Radioisotope Production: Diagnostic Radioisotopes and Monitor Reactions, vol. 1211. TECDOC, p. 49. IAEA. <http://www.nds.or.at/medical>.
- Tárkányi, F., Ditrói, F., Takács, S., Csikai, J., Hermanne, A., Uddin, M.S., Baba, M., 2016. Activation cross sections of proton induced nuclear reactions on palladium up to 80 MeV. Appl. Radiat. Isot. 114, 128–144.
- Tárkányi, F., Ditrói, F., Takács, S., Hermanne, A., Baba, M., Yuki, H., Ignatyuk, A.V., 2017. Investigation of activation cross sections of proton induced reactions on rhodium up to 70MeV for practical applications. Nucl. Instrum. Methods Phys. Res., Sect. B 412, 190–197.
- Tárkányi, F.T., Ignatyuk, A.V., Hermanne, A., Capote, R., Carlson, B.V., Engle, J.W., Kellett, M.A., Kibedi, T., Kim, G.N., Kondev, F.G., Hussain, M., Lebeda, O., Luca, A., Nagai, Y., Naik, H., Nichols, A.L., Nortier, F.M., Suryanarayana, S.V., Takacs, S., Verpell, M., 2019. Recommended nuclear data for medical radioisotope production: diagnostic gamma emitters. J. Radioanal. Nucl. Chem. 319, 487–531.
- Zaitseva, N.G., Ruratz, E., Vobecky, M., Hwan, K.H., Nowak, K., Tethal, T., Khalkin, V.A., Popinenkova, L.M., 1992. Excitation-function and yield for Ru-97 production in Tc-99 (P,3n)Ru-97 reaction in 20-100 Mev proton energy-range. Radiochim. Acta 56, 59–68.